The Cryosphere Discuss., https://doi.org/10.5194/tc-2018-197
Manuscript under review for journal The Cryosphere
Discussion started: 24 September 2018

The Cryosphere Discussions
Open Access
EGU

Assessment of Contemporary Satellite Sea Ice Thickness Products for Arctic Sea Ice

Heidi Sallila[1], Joshua McCurry[2,3], Sinéad Louise Farrell[2,3] and Eero Rinne[1]

[1]Finnish Meteorological Institute, Helsinki, Finland
[2]Cooperative Institute for Climate and Satellites, University of Maryland, College Park, MD, USA
[3]NOAA Laboratory for Satellite Altimetry, College Park, MD, USA

Correspondence to: Heidi Sallila (heidi.sallila@fmi.fi)

Abstract. Advances in remote sensing of sea ice over the past two decades have resulted in a wide variety of satellite-derived sea ice thickness data products becoming publicly available. Selecting the most appropriate product is challenging given objectives range from incorporating satellite-derived thickness information in operational activities, including sea ice forecasting, routing of maritime traffic, and search and rescue, to climate change analysis, longer-term modeling, prediction, and future planning. Depending on the use case, selecting the most suitable satellite data product can depend on the region of interest, data latency, and whether the data are provided routinely, for example via a climate or maritime service provider. Here we examine a suite of current sea ice thickness data products, collating key details of primary interest to end users. We assess sea ice thickness observations derived from sensors onboard the CryoSat-2 (CS2), Advanced Very-High-Resolution Radiometer (AVHRR) and Soil Moisture and Ocean Salinity (SMOS) satellites. We evaluate the satellite-only observations with independent ice draft and thickness measurements obtained from the Beaufort Gyre Exploration Project (BGEP) upward looking sonars (ULS) and Operation IceBridge, respectively. We find a number of key differences among data products, but find that products utilizing CS2-only measurements are reliable for sea ice between ~0.5 m and 4 m. Among those compare, a blended CS2-SMOS product was the most reliable for thin ice. Ice thickness distributions at the end of winter appeared realistic when compared with independent ice draft measurements, with the exception of those derived from AVHRR. We noticed disagreement among the products in mean thickness trends especially in the winters of 2012–2013 and 2016–2017. Regional comparisons reveal large differences in ice thickness between products, particularly in the Kara Sea, an area of considerable ship traffic.

1 Introduction

With the observed decline in Arctic sea ice extent (Parkinson and Cavalieri, 2008; Markus et al., 2009; Perovich et al., 2018) and interests in the exploitation of regional natural resources, activities in the Arctic have increased, alongside concerns for the state of the ice cover. Given its remote location, seasonally-available sunlight, and inhospitable climate, remote sensing provides the only means to obtain routine, basin-scale, and sustained observations of the Arctic Ocean. Objectives for

exploiting satellite-derived observations of the polar oceans are broad, and include improving sea ice forecasts, monitoring trends and variability in the polar climate system, advancing long-term climate predictions and future planning, understanding changes in marine habitats for wildlife and fisheries, as well as supporting operational activities, including navigation, hazard monitoring, disaster response, search and rescue, and many commercial activities. Because of these objectives, interest in routine measurements of sea ice thickness has increased, and is concurrent with the availability of new satellite data products that are the direct result of advances in remote sensing over the past few decades.

Sea ice is a key component of the Earth's climate system, acting as an insulator between the ocean and atmosphere, and its importance is recognised by the Global Climate Observing System (GCOS) through its status as an Essential Climate Variable (ECV) (Belward and Dowell, 2016). Sea ice thickness is an important sub-variable of the sea ice ECV. Although sea ice extent has traditionally been the more exploited variable, sea ice thickness measurements are just as, if not more, important than extent, and are needed together with ice concentration to calculate sea ice volume, the best indicator of the changes in the Arctic ice cover (e.g., Laxon et al., 2013; Song, 2016). Even if ice extent would remain the same for consecutive years, if the thickness decreases, the ice will be less resilient and more unlikely to regain thickness, eventually leading to decreased extent. Furthermore, Laxon et al. (2013) speculated that lower ice thickness, and volume, may be a factor behind the recent record minimums of sea ice extent. One way to understand the complex interactions of sea ice and its sub-variables in the climate system is through models, and in turn models initialized with sea ice observations can be used to forecast future ice-cover conditions. Recently satellite estimates of sea ice thickness have been used for the first time in model initialisations, revealing great improvements in model predictions (Yang et al., 2014; Allard et al., 2018; Xie et al., 2018), and these studies emphasize the importance of careful selection of the initialisation product. There have been other model studies with observational products from non-satellite sources such as airborne campaigns (e.g., Lindsay et al., 2012). However this type of data has restrictions in spatial and temporal coverage, and needs interpolation to emulate Arctic wide coverage.

As a result of advances over two decades in remote sensing of Arctic sea ice, a wide variety of satellite sea ice thickness data products have become available to the scientific community. One of the most widely used thickness data sets derives from the radar altimeter flown on CryoSat-2, the only satellite currently operating that provides nearly full coverage of the Arctic Ocean (Laxon et al., 2013). Sea ice thickness is derived from carefully processed radar altimeter measurements of ice surface elevation (Laxon et al., 2013; Kurtz et al. 2014). Because of differing approaches to retrack radar altimeter waveforms, a variety of processing algorithms exist, resulting in an array of thickness data products (e.g., Laxon et al., 2013; Kurtz et al., 2014; Ricker et al. 2014; Price et al. 2015; Tilling et al., 2015, 2016). These products broadly agree in the spatial distribution and gradients of ice thickness across the Arctic Ocean, but differ in their absolute magnitude. In addition to the CryoSat-2-only ice thickness products, there are other products derived from passive microwave radiometer measurements, as well as

visible imagery, that offer additional information such as coverage in the marginal ice zone or detection of sea ice conditions during the Arctic summer (e.g., Kaleschke et al., 2012; Key and Wang, 2015; Ricker et al., 2017a).

Given the variety of data products that are now available, identifying the most suitable product depends on the end user requirements. Without knowledge, means, or time to compare the different products, the end user may not select the product most appropriate for their needs. Which satellite data product is the most suitable depends upon a variety of factors, including the end user's region of interest, and data product characteristics including spatial coverage, temporal and spatial resolution, accuracy and quality, as well as data availability and latency.

In this paper we review a set of publicly-available satellite-derived sea ice thickness products, and compare them side by side for the first time, outlining their key attributes which are of interest to potential end users and for a range of applications. We evaluate sea ice thickness estimates derived from observations collected by CryoSat-2 (CS2), the Advanced Very-High-Resolution Radiometer (AVHRR), and the Soil Moisture and Ocean Salinity satellite (SMOS). We compare data product attributes and assess differences across products both from a regional and seasonal perspective, across the central Arctic Ocean and peripheral seas (Figure 1). We also evaluate the satellite data products, through comparisons with independent thickness measurements obtained in situ. There are several airborne and in situ observations suitable for validating the satellite measurements. Flight campaigns, such as Operation IceBridge (OIB) and CryoVEx, complement, and are used to evaluate, NASA's Ice Cloud and Elevation Satellite (ICESat) and CryoSat-2 observations, respectively. Comprehensive datasets covering a wide variety of Arctic variables are available from field measurements obtained during research cruises like the Norwegian young sea ice expedition (N-ICE2015), or the Multidisciplinary drifting Observatory for the Study of Arctic Climate (MOSAIC), planned to commence in October 2019. Also, a good set of observational products are available from North Polar drifting stations, ice mass balance buoys, upward looking sonars (ULS) that form part of the Beaufort Gyre Exploration Project (BGEP) and airborne EM measurements gathered through the Canadian Arctic Sea Ice Mass Balance Observatory campaign (see for example further information in Ricker et al., 2017b and Allard et al., 2018). For our evaluations we make use of OIB and ULS observations, which provide thickness and ice draft, respectively, since these variables are most compatible with the satellite data, and their records are more extensive and sustained over the period of interest, compared to many of the other publicly available in situ data sets.

The paper is structured as follows: section 2 introduces the sea ice thickness products and the independent data sets used for validation. Section 3 describes the methods used for product comparison. In section 4 we present the results of the comparisons across satellite products, and a product evaluation against independent estimates of ice thickness obtained from in situ and airborne sensors. We provide a summary discussion in section 5. In section 6 we conclude with a look ahead and provide recommendations for future satellite-derived thickness products aimed at addressing operational needs.

The Cryosphere Discuss., https://doi.org/10.5194/tc-2018-197
Manuscript under review for journal The Cryosphere
Discussion started: 24 September 2018

2 Data

2.1 Satellite Data Products for Arctic Sea Ice Thickness

Here we assess six contemporaneous sea ice thickness data products, derived from satellite measurements. Since our focus is an assessment of product utility for a range of operational activities we required that data products were open access, had basin-wide coverage of the Arctic Ocean, and were available for the majority of the time period under investigation. Four of these products comprise CS2-only thickness estimates, and include the Centre for Polar Observation and Modeling (CPOM) seasonally-averaged thickness product (Laxon et al., 2013), the Alfred Wegener Institute (AWI) version 2 monthly thickness product (Ricker et al., 2014), the NASA Jet Propulsion Laboratory (JPL) monthly thickness product (Kwok and Cunningham, 2015) and the NASA Goddard Space Flight Center (GSFC) 30-day thickness product (Kurtz and Harbeck, 2017). For comparison with CS2-only thickness estimates, we also consider blended CS2 - Soil Moisture Ocean Salinity (CS2SMOS) weekly ice thickness data (Ricker et al., 2017a), and the NOAA Climate Data Record (CDR) Extended Advanced Very High Resolution Radiometer (AVHRR) Polar Pathfinder (APP-x) daily ice thickness product. Further details about each data product are provided below. Common characteristics including measurement technique, temporal and spatial coverage, latency, frequency, resolution, and algorithm-specific details, are outlined in Table 1. The products selected for assessment provide a representative sample of available sources. We do however acknowledge that the list of satellite-derived ice thickness products is not exhaustive and other sources of similar observations exist. For example two additional sources of CS2-only sea ice data are now publicly available, one from the ESA Climate Change Initiative (CCI) and a second from the Laboratoire d'Études en Géophysique et Océanographie Spatiales (LEGOS) Center for Topographic studies of the Ocean and Hydrosphere (CTOH). Sea ice age characterization, and ice thickness, from the Visible Infrared Imager Radiometer Suite (VIIRS) instrument on the Suomi National Polar-orbiting Partnership (S-NPP) satellite, may also be derived in a similar manner to the APP-x data product (Key et al., 2013). These products were not included in this study since data were not publicly available at the time of writing, or required prior registration and approval with the data product provider. Since our focus is the availability of current sea ice thickness measurements for end users, our study period ranges 2010–2018, facilitating an assessment of recent sea ice conditions in the Arctic Ocean. Thus we do not consider satellite thickness records prior to the launch of CS2, such as from Envisat or ICESat.

2.1.1 CPOM

CPOM was first to produce publicly-available estimates of sea ice thickness from CS2 and they provide both near real time (NRT) thickness products for 28, 14, and 2-day observation periods (Tilling et al., 2016), which are updated on a daily basis with a typical latency of 3 days, as well as a seasonally-averaged thickness data product (Laxon et al., 2013) that is available

for two seasonal periods only (October–November and March–April, Table 1). Archived data coverage begins in March 2011, and new seasonal averages are available on an ad-hoc basis. Thickness data are available for the months of October through April on a 5 km grid for the full northern hemisphere (regions 1–14, Fig. 1), as well as on a 1 km grid for specific subpolar regions.

The basis for estimates of ice freeboard, and ultimately thickness, in the CPOM data product is level 1b CS2 waveforms, available from the European Space Agency (ESA) that are used to identify lead and ice floe elevations (Laxon et al., 2013). The mean scattering horizon of each waveform is identified through a threshold-first-maximum-retracking algorithm (TFMRA) with the threshold set at 70% of the power of the first maximum (Laxon et al., 2013). Leads and ice floes are distinguished using fixed criteria for stack kurtosis, stack standard deviation, and pulse peakiness. The CPOM algorithm utilizes the UCL13 mean sea surface (MSS) for the calculation of sea surface height anomalies, and to reduce the impact of geoid slope on freeboard estimates. This step is especially important in areas of low lead fraction (Skourup et al., 2017). Auxiliary information including the location of the ice edge and a product distinguishing first-year ice (FYI) from multi-year ice (MYI) is needed in the thickness algorithm. For sea ice concentration the NSIDC Near-Real-Time DMSP SSMIS Daily Polar Gridded Sea Ice Concentrations are used and the sea ice type is derived from the EUMETSAT's Ocean and Sea Ice Satellite Application Facility (OSI-SAF) product (Tilling et al., 2016).

2.1.2 AWI

AWI also provides monthly CS2 data products for October through April. Archived data begins in November 2010 and new monthly data are made available on a variable basis, but typically with one month latency (Table 1). In addition to thickness, AWI offers a number of additional geophysical and instrument parameters in their data product, including sea ice freeboard. It is the only product that provides uncertainty estimates for thickness and freeboard values (Hendricks et al., 2016). All parameters are provided on a 25 km grid for all regions of the Arctic (i.e., regions 1–14).

The algorithm employed by AWI does not differ significantly from that used in the derivation of the CPOM product, although AWI currently uses the DTU15 MSS for the calculation of sea surface height anomalies (Hendricks et al., 2016). Skourup et al. (2017) demonstrated that processing with either the DTU15 or UCL13 MSS results in consistent freeboard estimates, with only small deviations in areas of low lead concentration. For both sea ice concentration and type, AWI uses OSI-SAF products (Hendricks et al., 2016).

2.1.3 JPL

The JPL product provides monthly CS2 thickness data from January 2011 to December 2015, on a 25 km grid (Table 1). Coverage is limited geographically to the central Arctic (regions 1–6). Information on the ice concentration threshold defining the area within which sea ice thickness data are calculated is not provided. The JPL retracker for deriving surface elevation is based on the waveform centroid, rather than a leading-edge approach used in the AWI TFMRA algorithm. The JPL freeboard algorithm also uses the EGM2008 geoid, rather than a MSS model, which can result in anomalous sea ice thickness estimates in areas of steep ocean topography, such as near the Lomonosov and Gakkel Ridges (Skourup et al., 2017). The data are currently only accessible to the public after registration on a product website. Information about which sea ice concentration product is applied in the JPL algorithm is not provided in the available literature, but Kwok and Cunningham (2015) state that the sea ice type is derived from analysed fields of Advanced Scatterometer (ASCAT) data.

2.1.4 GSFC

GSFC provides 30-day ice thickness averages derived from CS2. Coverage begins in October 2010 and new data continue to be made available on a time-varying basis, but typically with a six week latency (Table 1). In addition to ice thickness, the GSFC product includes estimates of freeboard and surface roughness (Kurtz and Harbeck, 2017). All parameters are available on a 25 km grid, for regions 1–8.

Unlike other CS2 freeboard algorithms, the GSFC product is derived using a waveform-fitting method based on empirical calculation of expected returns from various surface types. Received waveforms are matched to a pre-calculated waveform by means of a least squares error minimization. Kurtz et al. (2014) note that this approach should nominally result in freeboard values lower than those derived from TFMRA-based methods. Additionally, the GSFC algorithm utilizes the DTU10 MSS for freeboard calculation. Skourup et al. (2017) have demonstrated that more recent MSS models (e.g., UCL13, DTU15), that incorporate sea surface height data from CS2, enhance the definition of gravity features, resulting in a more accurate freeboard derivation. Indeed Skourup et al. (2017) found that the DTU10 MSS in particular was not sufficient for freeboard processing due to decimeter-level discontinuities at 81.5°N and 86°N as well as at the ice edge, which resulted in erroneous freeboard measurements at these locations. An additional unique attribute of the GSFC algorithm is the use of a single density value (915 kg/m3) for all ice types in the thickness derivation step (Kurtz et al., 2014). In the case of the other CS2-only thickness products a dual density approximation is made, with the assumption of a lower density for MYI (882.0 kg/m3) than for FYI (916.7 kg/m3). Despite using a single density for both ice types, the GSFC algorithm employs a snow depth correction to the Warren et al. (1999) climatology for seasonal ice, as described in Laxon et al., (2013) and determined from OIB snow depth measurements provided in Kurtz and Farrell (2011). This approach is consistent with all other CS2 thickness products (Table 1). For sea ice concentration GSFC uses the NSIDC Near-Real-Time DMSP SSMI/S Daily Polar Gridded Sea Ice Concentrations and the OSI-SAF product for sea ice type (Kurtz and Harbeck, 2017).

2.1.5 CS2SMOS

The CS2SMOS sea ice thickness product, developed by AWI and the University of Hamburg, is a blended product of thickness estimates from CS2 and SMOS. It provides weekly data for the Arctic northward of 50 °N on an EASE2 grid, with 25 km grid resolution, across regions 1–14. It is available for a period starting in January 2011, ending April 2017.

The SMOS mission provides L-band observations of brightness temperature, which may be used to derive ice thickness in areas where thin sea ice exists (Kaleschke et al., 2012). CS2 exploits radar altimetry to measure the difference in height between the snow/ice surface and sea surface, which is then used to derive sea ice thickness through the assumption of hydrostatic equilibrium. Since CS2 was designed to measure ice thicker than 0.5 m, it may be advantageous to blend CS2 estimates with complementary estimates from SMOS. Due to the satellites having different spatial and temporal coverage, optimal interpolation is used to merge the two data sets. The algorithm includes weighting the data based on the known uncertainties of the products and modelled spatial covariances (Ricker et al., 2017a). The CS2 product used is the AWI CS2 product with processor version 1.2 (Ricker et al., 2014, Hendricks et al. 2016) and the SMOS thicknesses are from the University of Hamburg processor version 3.1 (Tian-Kunze et al., 2014, Kaleschke et al., 2016). For sea ice concentration and type OSI-SAF Arctic daily products are used.

2.1.6 APP-x

The NOAA extended AVHRR Polar Pathfinder (APP-x) product provides sea ice thickness estimates, along with 18 other geophysical variables, in a climate data record (Key and Wang, 2015). Thickness estimates are available for both the Arctic and Southern Oceans, spanning 1982 to present. Data are provided twice daily, with a typical latency of approximately 4 days (Table 1). Year-round thickness estimates are available, including throughout the summer, and are provided on a 25 km grid. We note a gap in the thickness record at the time of writing for the period 8 March to 1 May 2017 and hence no APP-x data exists for spring 2017 in the following analyses.

Sea ice thickness estimates are derived from AVHRR satellite radiometer measurements using a one-dimensional thermodynamic model (OTIM), based on a surface energy budget equation (Key and Wang, 2015). Ice thickness is calculated as a function of solar radiation and surface heat fluxes, surface albedo, and transmittance, where the surface fluxes are calculated as a function of surface skin and air temperature, surface air pressure, relative humidity, ice temperature, wind speed, cloud cover and snow depth. Thus OTIM relies on the following input for the ice thickness calculation: percentage cloud cover, surface skin temperature, surface broadband albedo and surface shortwave radiation fluxes, of which the latter two are obtained for daytime retrievals only. Since sea ice dynamics are not included in the model, the thickness errors are larger where the ice surface is not smooth, i.e. in regions with pressure ridges, hummocks and melt ponds. Generally OTIM tends to overestimate ice thickness, in particular for thin ice (Wang et al., 2010). Then again, APP-x tends to underestimate

thick ice, as the energy budget approach is less sensitive for thick ice. Moreover since the satellite retrieves 2 m air temperature, ice surface temperature is derived from the 2 m measurement. Wang et al. (2010) state that the thickness estimates are more accurate for nighttime retrievals, when 2 m air temperature and ice surface temperature are closer, resulting in a smaller model error. For this reason, we chose the nighttime estimates to be used in our study. Wang et al. (2010) note that errors due to uncertainties in snow depth and cloud fraction are the primary sources of error in the OTIM thickness estimates. OTIM is applicable to other optical satellite data including observations from NASA's Moderate Resolution Imaging Spectroradiometer (MODIS) instrument and EUMETSAT's Spinning Enhanced Visible and Infrared Imager (SEVIRI) instrument (Wang et al., 2010). The sea ice concentration source for the APP-x product is Nimbus-7 SMMR and DMSP SSM/I data processed with the NASA Team Algorithm (Key and Wang, 2015). The sea ice type is converted from the reflectances measured directly by AVHRR.

2.2 Evaluation Data Sets

2.2.1 Beaufort Gyre Exploration Project

Since August 2003, the Beaufort Gyre Exploration Project (BGEP) has operated a series of moorings in the Beaufort Sea, which have included an upward looking sonar (ULS) instrument. From 2003 to 2014 the ULS instrument produced a range estimate every two seconds, increasing in frequency to once per second starting with the 2014–2015 deployment. By subtracting the ULS range estimate from instrument depth, draft is measured to an accuracy of +/- 0.05 m per individual measurement (Krishfield et al., 2006).

Here we utilize ULS draft measurements from three mooring locations (A, B, and D, Fig. 1) in the Beaufort Sea over the six-month period spanning November–April, for all years from 2011–2016. Since the ULS measures ice draft as floes drift across the mooring location, the data represent a high-resolution, time-varying measurement of many individual leads and ice floes, thus providing a more complete picture of the regional ice thickness distribution. The draft to thickness ratio is approximately 0.9 (e.g., Rothrock et al., 2008), but to accurately compute thickness from draft, knowledge of ice type, ice density and snow loading are required. Here we do not convert draft to thickness, since that would introduce additional uncertainties. Rather we use the characteristics of the ice draft distribution to evaluate the satellite-derived thickness distribution.

2.2.2 Operation IceBridge

Operation IceBridge was launched in 2009 to continue the collection of sea ice and land ice elevation measurements in the temporal gap between the end of the ICESat mission in 2009 and the launch of ICESat-2 in 2018 (Koenig et al., 2010). The mission includes an airborne altimeter, the Airborne Topographic Mapper (ATM), which provides high-resolution measurements of sea ice plus snow freeboard, and a snow radar instrument for derivation of snow depth (Newman et al.,

2014). Together these allow for estimation of sea ice thickness (e.g., Farrell et al., 2012; Kurtz et al., 2013). Thickness uncertainty associated with IceBridge estimates is approximately 0.66 m (Richter-Menge and Farrell, 2013). Here we make use of the IDCSI4 (spring 2011) and NSIDC-0708 (spring 2012–2017) IceBridge thickness products available at the National Snow and Ice Data Center - Distributed Active Archive Center website (Kurtz et al., 2015; Kurtz, 2016). Due to the geographical layout of airborne flight surveys, the majority of IceBridge measurements sample multi-year sea ice in the Canada Basin (e.g., Richter-Menge and Farrell, 2013).

3 Methodology

3.1 Satellite Product Intercomparison

In order to compare the satellite data products, all ice thickness datasets are regridded to a 5 km grid, using a nearest neighbour algorithm with a 50 km search radius. Seasonally-averaged thicknesses are computed for two periods: fall (October and November), and spring (March and April). Seasonal averages are only calculated using grid cells that contain valid thickness estimates for both months. This prevents the average from being biased by measurements taken at the beginning or end of an averaging period (i.e., measurements only available in one of the two months). For each product we also calculate a climatological mean ice thickness in the central Arctic (Fig. 1), averaged over the product record (as described in Table 1). Climatological means are calculated separately for the fall and spring seasons. For each season we then compute deviation from the climatological mean for each product.

We define the CPOM seasonally-averaged thickness product as the reference dataset against which the other products are compared. We therefore compute product differences as follows:

$$\Delta SIT = SIT_c - SIT_p \ , \quad (1)$$

where SIT_c is the CPOM sea ice thickness, SIT_p is the thickness of the product in question, and $\boldsymbol{\Delta}$SIT is the difference between the two. Correlation statistics are calculated utilizing grid cells in which both data sets contain thickness estimates. These grid cell pairs are used to compute the Pearson correlation coefficient (r), the product difference according to Eq. 1., and the standard deviation of this difference.

To evaluate spatial variations in thickness across products regional ice thickness averages are computed for the central Arctic Ocean and each peripheral sea (Table 2) using the polygons shown in Fig. 1, for both the fall and spring seasons. Due to the limited ice extent in fall, the availability of observations in some peripheral seas is not sufficient to calculate a robust regional average in October–November (or in the spring season in the case of the JPL and GSFC products due to their limited spatial coverage).

3.2 Satellite Product Evaluation

Since the BGEP moorings are tethered to the seafloor, ULS measurements are representative of all ice floes drifting over the mooring location. To facilitate comparison with the satellite data, we select all product data points within 200 km of the mooring, creating a comparison region centred on the mooring location. In order to avoid influence from areas outside the comparison region, we use the original satellite thickness data as provided, rather than the gridded data described in Section 3.1 above.

Both the ULS draft data and satellite thickness data within the comparison region are averaged over one month intervals from November to April. The correlation coefficient between each monthly-averaged remote sensing product and the average ULS measurements for same period is calculated for each mooring. Any individual ULS draft measurement thinner than 0.1 m is not included in the averaging, as these measurements may represent leads rather than ice floes (Krishfield et al., 2006; Krishfield et al., 2014). In the case of the CPOM product, only seasonally-averaged thickness data are available, so correlations with the ULS ice draft are based on seasonal averages, rather than monthly averages as described above.

The sea ice thickness data from Operation IceBridge consists of flightlines across the Canada Basin and the central Arctic Ocean. Following Laxon et al. (2013), data acquired during IceBridge spring campaigns were interpolated onto a 50 km grid and compared against the satellite thickness data for March–April, for all six products interpolated at the same grid cell locations, using a nearest neighbor algorithm with a 100 km search radius. This allows the calculation of thickness differences between each product and IceBridge, as follows:

$$\Delta SIT_{eval} = SIT_{oib} - SIT_{p} \ , \quad (2)$$

where SIT_{oib} is the Operation IceBridge sea ice thickness, SIT_p is the thickness of the product in question, and $\boldsymbol{\Delta}\ SIT_{eval}$ is the difference between the two. Using the gridded data, we also calculate correlation coefficients, and standard deviation between each product and the IceBridge thickness observations.

4 Results

Here we present, for the first time, a side-by-side comparison of a suite of available CS2-only products, alongside a blended CS2-SMOS (CS2SMOS) product and one altimetry-independent sea ice thickness product, APP-x. The results are presented in three parts. First we provide a review of Arctic sea ice thickness variability during the last eight years. Next we compare regional and temporal differences between the satellite products across the Arctic regions. Finally we evaluate the satellite-derived thicknesses through comparisons with independent measurements.

4.1 State of the Arctic Sea Ice Thickness

Seasonal ice thickness for fall and spring is shown in Fig. 2 for the period 2011–2017. Following the observed low summer sea ice minimum extents in 2011 and 2012 (Parkinson and Comiso, 2013), we find that the lowest ice thickness was recorded in fall 2011 and 2012 (Fig. 2a). The loss of multi-year ice in the summer of 2012 due to the record sea ice minimum resulted in an overall thinner ice cover during the following winter/spring (i.e. spring 2013), which is visible in Fig. 2b. Following a cool summer in 2013, survival of ice through the melt season resulted in a rebound in thickness in fall 2013, and thicker winter sea ice in spring 2014, which has persisted in the central Arctic for subsequent seasons. This finding is consistent with earlier results shown in Tilling et al. (2015), who also noted a slight recovery in 2013–2014 following low winter-time ice thickness in 2011 and 2012. The thickest ice at the end of winter was observed in 2014 (Fig. 2b) in a region stretching from northern Greenland near Kap Morris Jesup, to Banks Island in the Canadian Arctic Archipelago. This region of thick ice in the central Arctic has persisted throughout the following seasons. As of spring 2018 (not shown) the area of ice more than 3 meters thick adjacent to the northern coasts of Greenland and the Canadian Arctic Archipelago is still greater than that of Spring 2012 and 2013, although the spatial extent of this thick ice area has diminished since 2014. In multiple springs (2012, 2014, 2015, 2016) an outflow of thick ice extends from the southern Canada Basin into the southern Beaufort Sea, due to the dynamic action of the Beaufort Gyre circulation (Fig. 2b). While this band of thick sea ice is captured in all of the CS2 products, it is not as easy to identify in the CS2SMOS product, and does not appear in the APP-x product (Fig. 2b). This overall picture of the state of Arctic sea ice thickness over the last several years is consistent across the CS2-only products and the CS2SMOS blended product. Although the APP-x product captures the spatial gradient in thick to thin ice, from the northern coasts of Greenland and Canada to the Siberian coastline, respectively, the product does not resolve many of the major changes in sea ice thickness conditions in either the spring or fall.

4.2 Regional Differences

The satellite-derived thickness products differ in their regional coverage and the availability of thickness estimates across the northern hemisphere. APP-x has the most widespread coverage, although CPOM, AWI and CS2SMOS all provide thickness estimates in the sub-polar seas. The JPL product only provides estimates for regions 1–6, while the GSFC product provides estimates for regions 1–8 (Table 1, and Fig. 2). Three of the six products (AWI, CS2SMOS, and APP-x) resolve thin ice (<= 0.5 m) at the periphery of the ice pack (regions 3–7) during the fall, but only CS2SMOS and APP-x resolve thin ice in these regions in spring (Fig. 2b). In addition APP-x does not resolve the thicker ice of the central Arctic Ocean, as evident in the other products, especially in the fall.

Maps of differences in ice thickness across products, as defined in Eq. 1., are shown in Fig. 3, and distributions of the differences between products are provided in Fig. S1. Average regional ice thickness for each region of the Arctic (as defined in Fig. 1) over the period 2011–2017 is provided in Table 2. As expected, given strong consistencies in algorithmic

approach, the closest agreement across products is found between CPOM and AWI (Fig. 3, Fig. S1). The thickness estimates of these products have a correlation of 0.88 for both seasons and a mean difference of 0.02–0.03 m (Fig. 4). However, there are noticeable regional differences in mean thickness during the observation period (Table 2), for example in the Greenland Sea (0.42 m difference) and the Canadian Archipelago (0.53 m difference). From an Arctic-wide perspective, the mean thickness estimates in the JPL product also differ little from the CPOM product (0–0.02 m, Fig. 4) and are highly correlated with the CPOM product, 0.86 in spring and 0.83 in fall (Fig. 4). There are however differences in the spatial gradients of ice thickness (Fig. 3), particularly in the central Arctic Ocean, where the JPL product estimates thicker ice close to Greenland, and thinner ice near the North Pole, and along the Siberian shelf zone (see also Table 2). Of the CS2-only data products, Figure 3 demonstrates that the GSFC thickness product is the most dissimilar to the CPOM data, with thickness in both the fall and spring periods being higher on average, though with year-to-year spatial variation (Fig. 3). Mean ice thickness differences range from 0.08 to 0.27 m (Fig. 4), though despite these differences, the GSFC product is still highly correlated with the CPOM product, with correlations of 0.80 and 0.83 in the spring and fall, respectively (Fig. 4). The CS2SMOS product suggests thinner ice thicknesses than the CS2-only products, with mean differences of 0.27 to 0.60 m (Fig. 4) and differences increasing towards the ice edge. For example in the Barents Sea, average spring thickness for the period 2011–2017 was only 0.38 m, over a meter lower than the CPOM product suggests (Table 2). Only in the MYI zone in spring does the CS2SMOS product provide estimates of thicker ice in some years (Fig. 3b), though never for a whole region (Table 2). Despite its lower thickness estimates, the CS2SMOS product correlates well with CPOM, 0.84 and 0.86 in the spring and fall, respectively (Fig. 4). For the central Arctic, APP-x is consistently thicker in spring over FYI, and thinner across the MYI zone and the thick outflow along the northern coast of Greenland and Canada (Fig. 3b, Table 2). In the fall, the APP-x product contains mainly thinner ice for all regions (Table 2), except in 2011 in the Canada Basin, where the APP-x product suggests thicker ice than in the CPOM product, and in 2017 around the ice edge in regions 3–6 (Fig. 3a). With correlations of 0.38 and 0.53 in the spring and fall, respectively, APP-x thickness does not correlate well with the CPOM product (Fig. 4). We also note that in fall 2017 the APP-x product shows thickness data covering an area south of the typical ice edge in regions 8–10 (Fig. 2a). Anomalous data in this region may be due to errors in the sea ice concentration field (not shown). Ice concentration is passed to the APP-x product from the lower-level APP product.

4.3 Differences in Winter-time Growth Rates

We now consider the winter-time growth rates across the central Arctic. The evolution of monthly mean ice thickness during winter is shown in Figure 5 for the entire study period spanning fall 2010 to spring 2018. The results are dependent on the product availability (Table 1), and in the case of the CPOM product, only seasonal means are available. Monthly mean ice thickness (Fig. 5) in the central Arctic can differ by up to 1.2 m across products. As we might expect, AWI and CPOM are the most similar of the CS2-only products, having maximum difference of 0.1 m. Ice thickness in the JPL product differs very little from these two, most noticeably in January and February 2013 (0.2 m higher than AWI). Ice thickness in the GSFC product is almost constantly higher than the other CS2-only products, with fall sea ice thickness estimates beginning

each season up to 0.4 m thicker, before converging towards the other CS2-only products by the end of the winter growth season. In December 2012, February 2013 and January 2016 the GSFC product indicates a small (0.1 m) decrease in thickness, whereas CPOM and AWI have a constant upward trend within the ice growth period. It is interesting to note that the CS2SMOS product also suggests a temporary decrease in ice thickness in December 2012 and February 2013. CS2SMOS is consistently lower than CS2-only products for all months except October 2015 when it converges with the JPL product. Like GSFC, CS2SMOS does not exhibit a constant upward trend during the ice growth season, instead showing significant month-to-month variability. Indeed monthly mean sea ice thickness typically decreases from the previous month once or twice per growth season. APP-x has the highest growth rate (i.e. the smallest minimum and largest maximum thickness) exceeding the CS2-only products, and the ice cover can gain 2 m within the ice growth season. The strongest increase in the APP-x mean thickness takes place at the end of winter between February and April, when the ice grows by up to 1 m. This differs significantly from the winter-time evolution of the ice as shown in the CS2-only products, which suggest stability in ice thickness at the end of winter (March–April), with very little growth, likely due to the insulating properties of the overlying snow cover.

The year-to-year seasonal trends in central Arctic ice thickness (Fig. 6) are very coherent among the CS2-only products, with an increase from 2011 to 2014, followed by a slight decrease and then a levelling off in mean thickness. In fall 2016 and 2017 (Fig. 6a) there is a minor divergence between the CPOM and AWI products, but both suggest a slight upward trend in fall ice thickness. The GSFC product in fall (Fig. 6a) shows a similar year-to-year trend to the other CS2-only products, but is 0.2–0.4 m thicker on average. CS2SMOS appears to be about 0.3 m thinner than the CS2-only products, but follows a similar trend (Fig. 6a). The fall averages in the APP-x product are lower than for the other products (Fig. 6a), except in 2012, when the CS2SMOS product also suggests an average of ~1 m. The mean thickness trend of the APP-x product does not follow the one of the CS2 products, in particular for the 2012 and 2016 that have opposite directions for the trend line from the CS2 products.

In spring the central Arctic mean ice thickness differs little across the CS2-only products (Fig. 6b), with the strongest similarities again between the CPOM and AWI products. The CS2-only products show a drop in thickness in 2012 and 2013, followed by a slight recovery in 2014, preceding another drop in mean thickness. The exception is in 2017 when the GSFC product suggests an increase in thickness, and is over 0.2 m higher than the other CS2-only products. By spring 2018 ice thickness in the GSFC product has decreased and is once again in line with the AWI and CPOM estimates. During this period the CS2SMOS mean is lower than the other products, differing from the CS2-only products by up to 0.7 m. The mean thickness trend, however, follows that of the CS2-only products, except that the CS2SMOS product suggests that the recovery in thickness occurred in 2013 rather than in 2014 (Fig. 6b). APP-x estimates are higher than for the other products in spring with an almost constant mean thickness of ~2.5–2.6 m, and very little year-to-year variability. In 2014–2016 this is in line with the CS2-only mean (differing by only 0.2 m).

We have calculated the annual deviations from the overall central Arctic mean thickness for the period 2011–2017 (referred to as the climatological mean) and present the results in Table 3. The departure from the spring climatological means for all CS2-only data products was 0.23 m in spring 2013 (0.1 m in 2012), and 0.20 m thicker in 2014, which is much in line with the thickness increase shown in Figure 6b. The CS2-only products are similar in the direction of annual departures from the climatological mean except for GSFC in spring 2017, which shows a positive departure, whereas the CPOM and AWI product thicknesses are lower than their climatological means. A very similar pattern of departures can be seen for fall CS2-only thickness data. CS2SMOS and APP-x show no noticeable deviation from their fall climatological means, as previously observed in Figure 6b. For fall, APP-x shows again little variation, except for 2016, when it deviates by -0.21 m (see also Figure 6a). The record low ice thickness in fall 2011 and 2012 are also evident in the results shown in Table 3.

4.4 Comparison against Independent Observations

Next we consider the satellite-derived sea ice thickness products in the context of independent measurements from ULS and IceBridge to evaluate the utility of the satellite products for providing information on the full thickness distribution. As mentioned previously, the draft to thickness ratio is approximately 0.9 (Rothrock et al., 2008). Therefore we do not expect the modal thickness and draft to be equivalent, but we do expect the distributions to have the same characteristic shapes.

Histograms of the draft/thickness distributions are shown in Figure 7, and suggest that the CS2-only satellite products capture neither the thickest nor thinnest ice. This may in part be due to the fact that the satellite derived products have been averaged to 25 km, thus masking out the thinnest and thickest measurements per grid cell. Among the CS2-only products, the thickness distribution of the AWI product most closely aligns with the ULS draft distribution, while the GSFC thickness distribution exhibits the least agreement with the draft distribution. CS2SMOS thickness directly overlaps with ULS draft, implying that the CS2SMOS product underestimates ice thickness. APP-x has an exceptionally narrow thickness distribution that captures far less variation than CS2 thickness products and is inconsistent with the characteristic shape of the ULS ice draft distribution.

The correlations between the monthly-averaged, satellite-derived ice thickness and ULS ice draft are shown for the months of November through April for each of the three BGEP moorings. Figure 8 shows the correlation between monthly averages, which were further combined across years (e.g. November 2011–2016, December 2011–2016, etc.) in Fig. 8 to aid visualization. Since the comparisons in Figure 8 are again illustrating thickness against draft, data should optimally fall above the y=x line, when the ~0.9 draft to thickness ratio is considered. With this assumption, and considering the mean values as outlined in Table 4, AWI performs best, confirmed by high correlation values and with mean thickness values 0.2 m greater than draft. Although the best correlation values are recorded by the JPL product, the thickness values appear to be biased slightly high, when keeping the ~0.9 ratio as reference. Logically, the products with varying dependency to draft have

lower correlation values, CS2SMOS being the lowest, although with relatively good correlation values. CS2SMOS thickness is roughly 10% higher than draft for ice around 1m, but is lower than draft when draft is greater than 1.3 m, which suggests underestimation of thickness in CS2SMOS estimates across this range. GSFC has comparatively low correlation values, and is roughly 0.5 m thicker than draft. APP-x thickness is increasingly greater than the ULS drafts with 0.5 m difference to draft of 1 m and 0.9 m to draft of 1.5 m, suggesting that it is overestimating ice thickness at this draft range. APP-x hardly shows any deviation from its climatological mean at each mooring location (Table 4), but for other products years of ice gain and loss are visible.

Next, the satellite-derived thickness estimates for spring are compared with seven years of independent OIB thickness data (Fig. 9). The JPL product has the highest correlation (r=0.73). We note that this is slightly higher than the correlation value of 0.56 noted in Kwok and Cunningham (2015), who only considered data for March and April 2011–2012. Likewise, our correlation value of 0.67 between CPOM and OIB thickness is in line with results from Laxon et al. (2013), who found a value of 0.61 when assessing CS2 against the 2011 and 2012 OIB campaigns. Similar to the results observed with the ULS comparisons, the satellite products seem to be missing the thickest ice seen by the OIB measurements, but overall the agreement between the CS2 products and OIB is good. In terms of absolute differences, JPL and GSFC thickness estimates are both slightly higher on average than those of OIB by 0.07, whereas CPOM and AWI estimates are lower by 0.14 m and 0.13 m, respectively. APP-x has the smallest correlation of 0.54 and a peculiar vertical line in the scatterplot, where a majority of APP-x sea ice thickness estimates fall into a thickness category between 2.15 m and 2.25 m. Unlike other products, CS2SMOS produces thickness estimates that are significantly thinner than those of OIB, with an average difference of 0.66 m. Our findings, that for thinner ice, CS2SMOS differs less from the validation product, whereas for thicker ice it tends to underestimate thickness, are in line with previous validation studies (Ricker et al., 2017b) who evaluated CS2SMOS using observations from an airborne electromagnetic (AEM) induction thickness sounding device.

4.5 Ice Freeboard

Recall (from Section 2) that only two products provide freeboard estimates: AWI and GSFC. Figure 10 compares sea ice freeboard across these two products for spring and fall. Our assessment reveals a prevalence of negative freeboard estimates in the GSFC product that do not appear in the AWI product (Fig. 10). For the period October 2010 to April 2018, an average of 29.5 % of the freeboard measurements provided in the GSFC data product are negative, in contrast to 0.9 % of the freeboard measurements in the AWI product. Negative freeboard estimates in the GSFC product often correspond with significantly higher freeboards in the AWI product for the same grid cell locations. An example of the GSFC freeboard product for April 2014 is shown in Figure 10c and highlights the spatial prevalence of anomalous, negative freeboard estimates, especially in the Kara and Barents Seas, where negative values persist throughout the winter. However, we note that negative freeboard estimates also occur in the Beaufort, Chukchi and Greenland Seas. This suggests that some negative

estimates may be related to regional masking in the processing algorithm, or they could be due to the use of the DTU10 MSS in the ice thickness derivation (e.g. see Fig. 3 in Skourup et al., 2017).

Despite the high proportion of negative freeboard values in the GSFC product, it does not contain any negative thickness values. Closer examination of individual data points indicates that ice thickness in grid cells with negative freeboard values is not significantly lower than adjacent data points, suggesting that a filter may be applied to remove negative freeboard values before calculating ice thickness, and/or that ice thickness values are derived from interpolations across many grid cells.

We furthermore note that the AWI and CPOM data products are the only two data products that include negative sea ice thickness estimates. Approximately 0.8 % and 0.2 % of the thickness estimates are negative in the CPOM and AWI data products, respectively. The locations of negative ice thickness estimates for the month of April 2014 are shown in Figure S2, and are representative of the general pattern observed in other years of the study period. Negative data points are found along the ice edge (as defined by the ice concentration threshold, Table 1), suggesting that these thickness values are anomalous and are a result of edge effects in the sea surface height interpolation scheme.

5 Discussion

We expect thickness estimates across the CS2-only products to be similar, since their only difference should be due to the algorithmic approach. These expectations are borne out as can be seen in the basin-scale maps shown in Fig. 2. The CPOM and AWI products differ very little, while the JPL thickness estimates are also generally in close agreement. The GSFC product is among the products with thickest sea ice overall, particularly at the beginning of the growth season (Figs. 4, 5, 8), despite containing a very high percentage of negative freeboard values (Fig. 10). On the other hand, due to the inclusion of SMOS data, the CS2SMOS product is weighted for thinner ice, such that we expect overall thickness in this data product to be lower than in the CS2-only datasets. Since the APP-x relies on a thermodynamical model to derive thickness, Wang et al. (2010, 2016) state that the product is expected to perform best over level ice. We find that in fall, APP-x indeed has similar ice thickness to the CS2SMOS product, except over the thickest MYI in the central Arctic (Fig. 2a, Fig. 3a). In spring, however, APP-x appears to overestimate ice thickness across the entire Arctic Ocean (Fig. 2b, Fig. 3b).

We have shown that the CS2-only satellite data products include reliable estimates for sea ice between ~0.5–4 m thick, depending on the product. In general, all satellite products capture a realistic winter-time ice thickness distribution, when compared to independent ice draft measurements, as demonstrated in Figure 7, with the exception of APP-x, which does a very poor job at resolving thickness variations in the Beaufort Sea. Although the width of the CS2SMOS thickness distribution suggests that the product captures a range of ice thickness in the region, it underestimates the absolute ice

thickness (Fig. 7). This may be due to too strong a weighting on the SMOS observations relative to the CS2 data, and the impact is most clearly seen in the multi-year ice zone (Fig. 2), where the CS2SMOS data product is consistently lower than the CS2-only data sets.

However our results also show that no product adequately captures the thinnest sea ice in the thickness distribution at the end of winter (Fig. 7). The CS2-only products also do not resolve the thickness of sea ice less than 0.5 m thick, equivalent to freeboards of less than 0.05 m (Figs. 4, 7, 9, 10), and the CS2SMOS product is the most reliable product in this regard (Fig. 7, Fig. 9). Ricker et al. (2014) found that uncertainties in sea ice thickness estimates are large for CS2 in areas where ice is less than 1 m thick. In contrast, the sensitivity is lost for SMOS when the ice is thicker than 1 m. While we have demonstrated that CS2-only products provide good results in the central Arctic ice pack, they lack robust estimates around the ice margins, and in areas of new ice formation, where thin ice is expected. The opposite argument applies to the CS2SMOS product.

The biggest difference in the temporal trend among the thickness products occurs in spring 2013. While the CS2-only products show a drop in average Arctic ice thickness following the record September 2012 sea ice minimum, the CS2SMOS product continues to suggest overall thickening between 2012 and 2014 (Fig. 2, Fig. 5). In addition both GSFC and CS2SMOS products suggest a decrease in mean ice thickness for the central Arctic in both December 2012 and February 2013 (Fig. 5, Fig. 6). During spring 2013 significant episodes of ice divergence were reported, with observations of pronounced lead signals in the multi-year ice zone (Willmes and Heinemann, 2015). This may be one reason why the CS2SMOS product departs from the trends shown in the CS2-only products, but further study is needed to fully understand the impact of ice dynamics on the CS2SMOS product and differences between it and the CS2-only products. The CS2SMOS product also shows uneven growth and decline in the mean ice thickness each winter that could be due to changes in the extent of thin ice, if the assumption holds true that SMOS is too heavily weighting in the blended product. Another period with deviation from the overall trends was the ice season between fall 2016 and spring 2017. In October–November 2016 a decrease in the mean ice thickness can be seen in the APP-x product, and to very small extent also in the CS2SMOS and CPOM products, whereas in March–April 2017 the GSFC products shows an increase in mean ice thickness. The APP-x product did not resolve any year-to-year variability in mean thickness. During the ice growth season the APP-x product shows the largest magnitude of ice growth, over 1.5 m between fall and spring (Fig. 6), with very little inter-annual variability (Fig. 2, Fig. 5). The largest growth in the APP-x product occurs between February and April, at the end of winter (Fig. 5), when in situ measurements typically show inhibited ice growth due to the insulating effects of the overlying snow cover. This suggests that thermodynamic assumptions in the OTIM algorithm for the end of winter may need further refinement.

Finally, we also note that all of the satellite-derived sea ice thickness products depend on additional auxiliary data sets (Table 1) in the derivation of ice thickness. As we have outlined in Table 1, most use different sources for the mean sea surface model, ice type delineation, ice concentration, and the treatment of ice density and snow depth on ice. Comparing the auxiliary products is outside the scope of this study, but these could give rise to differences across products, in addition to the algorithmic differences. There is also a large range in the ice concentration threshold used to indicate the ice edge across products, varying from 15 % (in the APP-x and CS2SMOS products) to 75 % (in the CPOM product). With regards to the APP-x product we believe that an erroneous ice concentration threshold could be one possible explanation for the peculiar extent of the ice thickness estimates in fall 2017 (Fig. 2a).

6 Conclusions and Future Outlook

Satellite techniques have revolutionized our ability to measure the thickness of ice in the Arctic Ocean, providing critical information for scientists conducting studies of environmental change in the region, as well as a new source of data for forecasters, modelers, operators, and decision makers. Here we assessed a suite of existing satellite-derived, publicly-available, Arctic sea ice thickness data products, conducting a comprehensive examination of regional and seasonal differences. As expected, the CS2-only products were similar, particularly at the end of winter (Fig. 6b). In March/April of each year, APP-x reached a mean Arctic-wide thickness of 2.6 m, which was thicker than any other satellite product, and showed little to no inter-annual variability. On the other hand, because of its inclusion of thin sea ice thickness, derived from passive microwave radiometer data, the CS2SMOS data product is on average 1 m thinner than the other satellite estimates at the end of the winter growth season. In fall, there was a larger spread in mean thickness across the products, and the GSFC thickness product diverged from the three other CS2-only products by approximately 0.2–0.3 m (Fig. 6a). Evaluation of the satellite data products through comparisons with OIB and ULS measurements revealed that all products were well correlated with the independent ice draft/thickness estimates. Five of the six products resolved an accurate winter-time sea ice thickness distribution for the Beaufort Sea when compared with ULS observations of ice draft, though the AWI data set produced the most robust result. The APP-x data product did not resolve ice thickness variability in this region, and was biased thick compared to both the ULS ice draft observations and the alternative satellite thickness products. Our study revealed some other remarkable differences across the products utilizing CS2 data. Both the GSFC and CS2SMOS data products suggest reductions in Arctic mean ice thickness during the ice growth season. There was an unexpected increase in mean ice thickness in spring 2017 in the GSFC product that differed from the other CS2 products. There was also an upward mean ice thickness trend in spring 2013 in the CS2SMOS data product, when the CS2-only products showed a continued decrease in mean thickness. Such anomalies require further study to evaluate their causes, and this can be accomplished for example through more detailed, along-orbit comparisons between CS2 data with coincident observations collected during OIB and CryoVex underflights (e.g., Connor et al., 2011).

In terms of end user applications, the suitability of a particular product depends on the region of interest, as well as data latency and availability. Moreover the purpose for which the data are used is critical in selecting the most suitable satellite product. For example climate assessments favour accuracy, while those engaged in operational or forecasting activities require low-latency, high-frequency observations. The frequency of the satellite data products evaluated here varies from twice a day (APP-x) to monthly (AWI), and latency varies from three / four days (APP-x and CPOM NRT) to products that are updated seasonally, or on an ad-hoc basis (GSFC and the CPOM seasonally-averaged thickness data product, Table 1). If access to NRT measurements, with year-round availability is required, APP-x would be the first choice, since it is the only product that provides daily coverage across the Arctic Ocean, and a reasonable measure of mean ice thickness. However, it does not resolve the cross-basin ice thickness gradient nor the location of the thickest ice. Should basin-scale gradients in ice thickness (i.e., the thickness distribution) be important to the end user, then the APP-x product is not recommended, and CPOM NRT product is preferable, although it is only available for the winter-growth season (Tilling et al., 2016). In terms of climatological studies, or model initialization and hindcast studies, the CS2-only data products are appropriate options, but for navigation in the Arctic, none of these products are suitable as a single source of information, and the utility of the observations would only be realised when combined with additional ice charting analyses.

A remaining challenge for the satellite-derived thickness products is the treatment of snow depth on sea ice. We do not have a reliable data source that provides observations of the interannual variability of snow (Blanchard-Wrigglesworth et al., 2018). Most of the satellite-derived thickness products assessed here make use the modified Warren et al. (1999) snow climatology (as outlined in Laxon et al., 2013), which does not resolve year-to-year variations in snow depth. The need for improved knowledge of snow depth holds especially true for the APP-x, wherein a uniform 0.20 m snow cover is currently assumed (Key and Wang, 2015), which we expect contributes to the poor reproduction of variability in thickness gradients across the central Arctic, and exceptional ice growth at the end of winter. There are currently multiple approaches proposed to obtain seasonal snow estimates, though these have yet to be routinely incorporated into a publicly-available satellite thickness data product. Potential solutions include utilizing model simulations (e.g., Blanchard-Wrigglesworth et al., 2015), atmospheric reanalysis data (e.g., Blanchard-Wrigglesworth et al., 2018), extrapolating in situ observations (e.g. Shalina and Sandven, 2018), or widely expanding the spatial and temporal coverage of current airborne snow depth measurement techniques (e.g. Kurtz and Farrell, 2011; King et al., 2015). Satellite passive microwave radiometer observations have also been used to derived snow on first-year sea ice (Brucker and Markus, 2013), as well as snow on thick ice (Maass et al., 2012). One additional promising remote-sensing method is to combine two satellite altimeter observations retrieved at different wavelengths, enabling snow retrieval due to differences in penetration (Shepherd et al., 2018). For example this could be achieved through a combination of dual-band radar freeboard observations (e.g. Guerreiro et al., 2016) or by comparing freeboard measurements from ICESat-2 with CryoSat-2, or Sentinel-3, to obtain an estimate of year-to-year changes in snow depth (e.g., Kwok and Markus, 2017).

In light of the current challenges presented by the treatment of snow in the existing data products, a selection of end users, particularly those conducting data assimilation experiments, are interested in sea ice freeboard, rather than ice thickness, since freeboard represents the remote sensing observation (rather than thickness which is a derivation). Currently there are only two products that provide the freeboard parameter, AWI and GSFC. Our analysis suggests that the AWI data set is preferable due to a more realistic representation of ice freeboard measurements across the Arctic (Fig. 10). We found a high prevalence of erroneous, negative freeboard estimates throughout the Arctic in the GSFC product, that were especially concentrated in the peripheral seas, particularly in regions 7 and 8, as well as in the Beaufort Sea. The source of these anomalies is most likely associated with aspects of the GSFC algorithm and interpolation of the mean sea surface between lead tie-points.

In conclusion we suggest that low-latency, monthly composites, derived from CS2 data, but updated daily with the latest-available measurements, would benefit many sea ice thickness applications and provide an ideal solution to address many end-user needs. Further, it may be possible to obtain a more robust thickness distribution, through the inclusion of passive microwave observations of thin-ice thickness in the marginal ice zone. Our results show however that applying an appropriate ratio, that adequately combines microwave and altimeter observations, is challenging and requires further evaluation with independent observations. Higher resolution (<= 5 km) along-orbit and gridded data products would advance the utility of the observations at the regional scale. We also recommend that future products include both ice thickness and freeboard parameters, as well as an estimate of thickness uncertainty and/or data quality flags, so that the satellite observations may be used in data assimilation experiments aimed at improving ice forecasting.

Author contribution

SLF designed the study, HS and JM carried out the data analysis under the guidance of SLF, and JM was responsible for producing the figures. HS led the manuscript preparation, and SLF, ER and JM contributed to the writing and internal review.

Competing interests

The authors declare that they have no conflicts of interest.

Acknowledgements

All data utilized in this study are publicly available and all data sources are listed in Table 1. This work has been funded through the ESA Sea Ice Climate Change Initiative (CCI) project and the NOAA Product Development, Readiness, and

Application (PDRA) / Ocean Remote Sensing (ORS) Program, under NOAA grant NA14NES4320003 (Cooperative Institute for Climate and Satellites, University of Maryland).

References

Allard, R. A., Farrell, S. L., Hebert, D. H., Johnston, W. F., Li, L., Kurtz, N. T., Phelps, M. W., Posey, P. G., Tilling, R., Ridout, A., and Wallcraft, A. L.: Utilizing CryoSat-2 sea ice thickness to initialize a coupled ice-ocean modeling system, Advances in Space Research, doi:10.1016/j.asr.2017.12.030, 2018.

Armitage, T. W. K and Ridout, A. L.: Arctic sea ice freeboard from AltiKa and comparison with CryoSat-2 and Operation IceBridge, Geophys. Res. Lett., 42, 6724–6731, doi::10.1002/2015GL064823, 2015.

Belward, A. and Dowell, M. (eds.): The Global Observing System for Climate (GCOS): Implementation Needs, GCOS 2016 Implementation Plan, Global Ocean Observing System Report (GCOS 200, GOOS 214), World Meteorological Organisation, 341, https://library.wmo.int/opac/doc_num.php?explnum_id=3417, 2016.

Blanchard-Wrigglesworth, E., Farrell, S., Newman, T., and Bitz, C.: Snow cover on Arctic sea ice in observations and an Earth system model, Geophysical Research Letters, 42, 10342–10348. https://doi.org/10.1002/2015GL066049, 2015.

Blanchard-Wrigglesworth, E., Webster, M. A., Farrell, S. L. and Bitz, C. M.: Reconstruction of Snow on Arctic Sea Ice, Journal of Geophysical Research: Oceans, 123(5), 3588-3602, doi:https://doi.org/10.1002/2017JC013364, 2018.

Brucker, L., and Markus, T.: Arctic-scale assessment of satellite passive microwave-derived snow depth on sea ice using Operation IceBridge airborne data, J. Geophys. Res. - Oceans, 118, 2892–2905, doi:10.1002/jgrc.20228, 2013.

Connor L. N., Laxon S. W., McAdoo D. C., Ridout A., Cullen R., Farrell S., and Francis R.: Arctic sea ice freeboard from CryoSat-2: Validation using data from the first IceBridge underflight, AGU Fall Meeting Abstracts, 2011.

Farrell, S. L., Kurtz, N., Connor, L. N., Elder, B. C., Leuschen, C., Markus, T., McAdoo, D. C., Panzer, B., Richter-Menge, J., and Sonntag, J.G.: A first assessment of IceBridge snow and ice thickness data over Arctic sea ice, IEEE Transactions on Geoscience and Remote Sensing, 50(6), 2098-2111, 2012.

Grosfeld, K., Treffeisen, R., Asseng, J., Bartsch, A., Bräuer, B., Fritzsch, B., Gerdes, R., Hendricks, S., Hiller, W., Heygster, G., Krumpen, T., Lemke, P., Melsheimer, C., Nicolaus, M., Ricker, R. and Weigelt, M.: Online sea-ice knowledge and data

platform <www.meereisportal.de>, Polarforschung, Bremerhaven, Alfred Wegener Institute for Polar and Marine Research & German Society of Polar Research, 85 (2), 143-155, doi:10.2312/polfor.2016.011, 2016.

Guerreiro, K., Fleury, S., Zakharova, E., Rémy, F., and Kouraev, A.: Potential for estimation of snow depth on Arctic sea ice from CryoSat-2 and SARAL/AltiKa missions, Remote Sensing of Environment, 186, 339-349, doi:10.1016/j.rse.2016.07.013, 2016.

Hendricks, S., Ricker, R., and Helm, V.: User Guide - AWI CryoSat-2 Sea Ice Thickness Data Product (v1.2), 10013/epic.48201, 2016.

Kaleschke, L., Tian-Kunze, X., Maaß, N., Beitsch, A., Wernecke, A., Miernecki, M., Müller, G., Fock, B. H., Gierisch, A. M. U., Schlünzen, K. H., Pohlmann, T., Dobrynin, M., Hendricks, S., Asseng, J., Gerdes, R., Jochmann, P., Reimer, N., Holfort, J., Melsheimer, C., Heygster, G., Spreen, G., Gerland, S., King, J., Skou, N., Søbjærg, S. S., Haas, C., Richter, F., and Casal, T.: SMOS sea ice product: Operational application and validation in the Barents Sea marginal ice zone, Remote Sensing of Environment, 180, 264 – 273, doi:10.1016/j.rse.2016.03.009, 2016.

Kaleschke, L., Tian-Kunze, X., Maaß, N., Makynen, M., & Drusch, M.: Sea ice thickness retrieval from SMOS brightness temperatures during the Arctic freeze-up period. Geophysical Research Letters, 39: L05501. doi:10.1029/2012GL050916, 2012.

Key, J. R., R. Mahoney, Y. Liu, P. Romanov, M. Tschudi, I. Appel, J. Maslanik, D. Baldwin, X. Wang and P. Meade: Snow and ice products from Suomi NPP VIIRS, J. Geophys. Res. Atmos., 118, 12,816–12,830, doi:10.1002/2013JD020459, 2013.

Key, J. and Wang, X.: Extended AVHRR Polar Pathfinder (APP-x) Climate Algorithm Theoretical Basis Document, NOAA Climate Data Record Program, CDRP-ATBD-0573, 01B-24b, Rev. 1, 82, 2015.

King, J., Howell, S., Derksen, C., Rutter, N., Toose, P., Beckers, J. F., Haas, C., Kurtz, N. and Richter-Menge, J.: Evaluation of Operation IceBridge quick-look snow depth estimates on sea ice, Geophysical Research Letters, 42(21), 9302-9310, 2015.

Koenig, L., Martin, S., Studinger, M., and Sonntag, J.: Polar airborne observations fill gap in satellite data, Eos, Transactions American Geophysical Union, 91(38), 333-334, 2010.

Krishfield, R. A. and Proshutinsky, A.: BGOS ULS Data Processing Procedure. Woods Hole Oceanographic Institute report, available at: http://www.whoi.edu/fileserver.do?id=85684&pt=2&p=100409, last access 26 April 2018, 2006.

Krishfield, R.A., Proshutinsky, A., Tateyama, K., Williams, W.J., Carmack, E.C., McLaughlin, F.A. and Timmermans, M.L.: Deterioration of perennial sea ice in the Beaufort Gyre from 2003 to 2012 and its impact on the oceanic freshwater cycle, Journal of Geophysical Research: Oceans, 119(2), 1271-1305, 2014.

Kurtz, N. T., and S. L. Farrell: Large-scale surveys of snow depth on Arctic sea ice from operation IceBridge, Geophys. Res. Lett., 38, L20505, doi:10.1029/2011GL049216, 2011.

Kurtz, N. T., Farrell, S. L. , Studinger, M., Galin, N., Harbeck, J. P., Lindsay, R., Onana, V. D., Panzer, B., and Sonntag, J. G.: Sea ice thickness, freeboard, and snow depth products from Operation IceBridge airborne data. The Cryosphere, 7, 1035-1056,
doi:10.5194/tc-7-1035-2013, 2013.

Kurtz, N. T., Galin, N., and Studinger, M.: An improved CryoSat-2 sea ice freeboard retrieval algorithm through the use of waveform fitting, The Cryosphere, 8, 1217-1237. doi:10.5194/tc-8-1217-2014, 2014.

Kurtz, N., Studinger, M., Harbeck, J., Onana, V., and Yi, D.: IceBridge L4 Sea Ice Freeboard, Snow Depth, and Thickness, Version 1 [March–April 2011], NASA National Snow and Ice Data Center Distributed Active Archive Center, Boulder, Colorado USA, [accessed 2018], doi:10.5067/G519SHCKWQV6, 2015.

Kurtz, N. and Harbeck, J.: CryoSat-2 Level-4 Sea Ice Elevation, Freeboard, and Thickness, Version 1 [October–April, 2010–2018], NASA National Snow and Ice Data Center Distributed Active Archive Center, Boulder, Colorado USA, [accessed 2018], doi:10.5067/96JO0KIFDAS8, 2017.

Kurtz, N.: IceBridge Sea Ice Freeboard, Snow Depth, and Thickness Quick Look, Version 1 [March–April, 2012–2017], NASA National Snow and Ice Data Center Distributed Active Archive Center, Boulder, Colorado USA, [accessed 2018], doi:10.5067/GRIXZ91DE0L9, 2016.

Kwok, R. and Markus, T.: Potential Basin-Scale Estimates of Arctic Snow Depth with Sea Ice Freeboards from CryoSat-2: An Exploratory Analysis, Adv. Space Res., doi:10.1016/j.asr.2017.09.007, 2017.

Laxon S. W., Giles, K.A., Ridout, A. L., Wingham, D.J., Willatt, R., Cullen, R., Kwok, R., Schweiger, A., Zhang, J., Haas, C., Hendricks, S., Krishfield, R., Kurtz, N., Farrell, S. and Davidson, M.: CryoSat-2 estimates of Arctic sea ice thickness and volume, Geophys. Res. Lett., 40, 732–737, doi:10.1002/grl.50193, 2013.

Lindsay, R., Haas, C., Hendricks, S., Hunkeler, P., Kurtz, N., Paden, J., Panzer, B., Sonntag, J., Yungel, J., Zhang, J.: Seasonal forecasts of Arctic sea ice initialized with observations of ice thickness, Geophys. Res. Lett., 39, L21502, doi:10.1029/2012GL053576, 2012.

Markus, T., Stroeve, J. C., and Miller, J.: Recent changes in Arctic sea ice melt, onset, freezeup, and melt season length, J. Geophys. Res., 114, C12024, doi:10.1029/2009JC005436, 2009.

Maaß, N., Kaleschke, L., Tian-Kunze, X., and Drusch, M.: Snow thickness retrieval over thick Arctic sea ice using SMOS satellite data, The Cryosphere, 7, 1971-1989, https://doi.org/10.5194/tc-7-1971-2013, 2013.

Newman, T., Farrell, S. L., Richter-Menge, J., Connor, L. N., Kurtz, N. T., Elder, B. C. and McAdoo, D.: Assessment of radar-derived snow depth over Arctic sea ice, Journal of Geophysical Research: Oceans, 119(12), 8578-8602, 2014.

Parkinson, C.L., and Cavalieri, D.J.: Arctic sea ice variability and trends, 1979-2006, J. Geophys. Res., 113, C07003. doi:10.1029/2007JC004558, 2008.

Parkinson, C.L., and Comiso, J.C.: On the 2012 record low Arctic sea ice cover: Combined impact of preconditioning and an August storm, Geophys. Res. Lett., doi:10.1002/grl.50349, 2013.

Perovich, D. K., Meier, W., Tschudi, M., Farrell, S., Hendricks, S., Gerland, S., Haas, C., Krumpen, T., Polashenski, C., Ricker, R. and Webster, M.: Sea ice cover [in "State of the Climate in 2018"], Bull. Amer. Meteor. Soc., 99(8), S147–152, doi:10.1175/2018BAMSStateoftheClimate.1., 2018.

Price, D., Beckers, J., Ricker, R., Kurtz, N., Rack, W., Haas, C., Helm, V., Hendricks, S. Leonard, G., and Langhorne, P. J.: Evaluation of CryoSat-2 derived sea-ice freeboard over fast ice in McMurdo Sound, Antarctica, J. Glaciol. 61 (226), doi:10.3189/2015JoG14J157, 2015.

Richter-Menge, J. A., and Farrell, S. L.: Arctic sea ice conditions in spring 2009–2013 prior to melt, Geophys. Res. Lett., 40, 5888–5893, doi:10.1002/2013GL058011, 2013.

Ricker, R., Hendricks, S., Helm, V., Skourup, H., and Davidson, M.: Sensitivity of CryoSat-2 Arctic sea-ice freeboard and thickness on radar-waveform interpretation, The Cryosphere, 8 (4), 1607-1622, doi:10.5194/tc-8-1607-2014, 2014.

Ricker, R., Hendricks, S., Kaleschke, L., and Tian-Kunze, X.: CS2SMOS User Guide v3.0, Alfred Wegener Institute, 10013/epic.51136, 2017a.

Ricker, R.; Hendricks, S.; Kaleschke, L.; Tian-Kunze, X.; King, J. and Haas, C.: A weekly Arctic sea-ice thickness data record from merged CryoSat-2 and SMOS satellite data, The Cryosphere, 11, 1607-1623, doi:10.5194/tc-11-1607-2017, 2017b.

Rothrock, D. A., Percival, D. B. and Wensnahan, M.: The decline in arctic sea-ice thickness: Separating the spatial, annual, and interannual variability in a quarter century of submarine data, Journal of Geophysical Research: Oceans, 113(C5), 2008.

Shalina, E. V. and Sandven, S.: Snow depth on Arctic sea ice from historical in situ data, The Cryosphere, 12, 1867-1886, doi:10.5194/tc-12-1867-2018, 2018.

Shepherd, A., Fricker, H. A., and Farrell S. L.: Trends and connections across the Antarctic cryosphere, Nature, 558(7709), 223-232, 2018.

Skourup, H., Farrell, S. L., Hendricks, S., Ricker, R., Armitage, T. W. K., Ridout, A., Andersen, O. B., Haas, C., and Baker, S.: An assessment of state-of-the-art mean sea surface and geoid models of the Arctic Ocean: Implications for sea ice freeboard retrieval, Journal of Geophysical Research: Oceans, 122, 8593–8613, doi:10.1002/2017JC013176, 2017.

Song, M.R.: Change of Arctic sea ice volume and its relationship with sea ice extent in CMIP5 simulations, Atmospheric and Oceanic Science Letters, 9, 22–30, doi:10.1080/16742834.2015.1126153, 2016.

Tian-Kunze, X., Kaleschke, L., Maaß, N., Mäkynen, M., Serra, N., Drusch, M., and Krumpen, T.: SMOS-derived thin sea ice thickness: algorithm baseline, product specifications and initial verification, The Cryosphere, 8, 997–1018, doi:10.5194/tc-8-997-2014, URL http://www.the-cryosphere.net/8/997/2014/, 2014.

Tilling, R.L., Ridout, A., Shepherd, A., and Wingham, D.J.: Increased Arctic sea ice volume after anomalously low melting in 2013, Nature Geoscience, 8(8), 643, doi:10.1038/NGEO2489, 2015.

Tilling, R.L., Ridout, A., and Shepherd, A.: Near-real-time Arctic sea ice thickness and volume from CryoSat-2, The Cryosphere, 10(5), 2003-2012, 2016.

Wang, X., Key, J. R., and Liu, Y.: A thermodynamic model for estimating sea and lake ice thickness with optical satellite data, J. Geophys. Res., 115, C12035, doi:10.1029/2009JC005857, 2010.

Wang, X., Key, J., Kwok, R., and Zhang, J.: Comparison of Arctic Sea Ice Thickness from Satellites, Aircraft, and PIOMAS Data, Remote Sens., 8, 713, 2016.

Warren, S. G., Rigor, I. G., Untersteiner, N., Radionov, V. F., Bryazgin, N. N., Aleksandrov, Y. I., and Colony, R.: Snow depth on Arctic sea ice, J. Clim., 12, 1814–1829, 1999.

Willmes, S. and Heinemann, G.:. Sea-Ice Wintertime Lead Frequencies and Regional Characteristics in the Arctic, 2003-2015, Remote Sens., 8(1), 4; doi:10.3390/rs8010004, 2015.

Wingham, D. J., Francis, C. R., Baker, S., Bouzinac, C., Brockley, D., Cullen, R., de Chateau-Thierry, P., Laxon, S. W., Mallow, U., Mavrocordatos, C., Phalippou, L., Ratier, G., Rey, L., Rostan, F., Viau, P., and Wallis, D. W.: CryoSat: A mission to determine the fluctuations in Earth's land and marine ice fields, Adv. Space Res., 37, 841–871, doi:10.1016/j.asr.2005.07.027, 2006.

Xie, J., Counillon, F., and Bertino, L.: Impact of assimilating a merged sea ice thickness from CryoSat-2 and SMOS in the Arctic reanalysis, The Cryosphere Discuss., doi:10.5194/tc-2018-101, in review, 2018.

Yang, Q., Losa, S. N., Losch, M., Tian-Kunze, X., Nerger, L., Liu, J., Kaleschke, L., and Zhang, Z.: Assimilating SMOS sea ice thickness into a coupled ice-ocean model using a local SEIK filter, J. Geophys. Res. Oceans, 119, 6680-6692, doi:10.1002/2014JC009963, 2014.

The Cryosphere Discuss., https://doi.org/10.5194/tc-2018-197
Manuscript under review for journal The Cryosphere
Discussion started: 24 September 2018

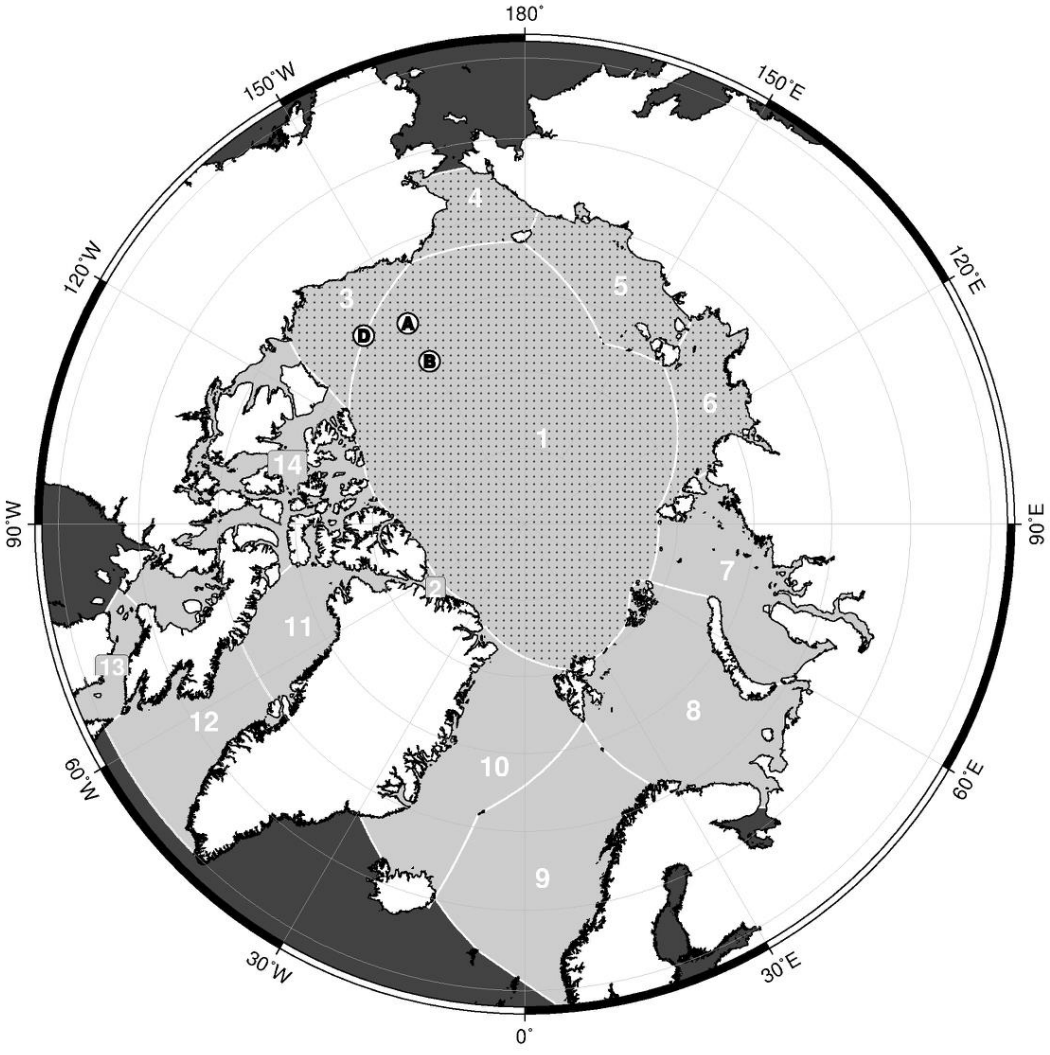

Figure 1: Regions utilised in data analysis: (1) Central Arctic Ocean, (2) Lincoln Sea, (3) Beaufort Sea, (4) Chukchi Sea, (5) East Siberian Sea, (6) Laptev Sea, (7) Kara Sea, (8) Barents Sea, (9) Norwegian Sea, (10) Greenland Sea, (11) Baffin Bay, (12) Davis Strait, (13) Hudson Strait, and (14) Canadian Arctic Archipelago. The dotted area represents the central Arctic region (1–6) within which all data products are available. The locations of Beaufort Gyre Exploration Project (BGEP) moorings A, B, and D are also indicated (white circles with mooring designation).

The Cryosphere Discuss., https://doi.org/10.5194/tc-2018-197
Manuscript under review for journal The Cryosphere
Discussion started: 24 September 2018

(a)

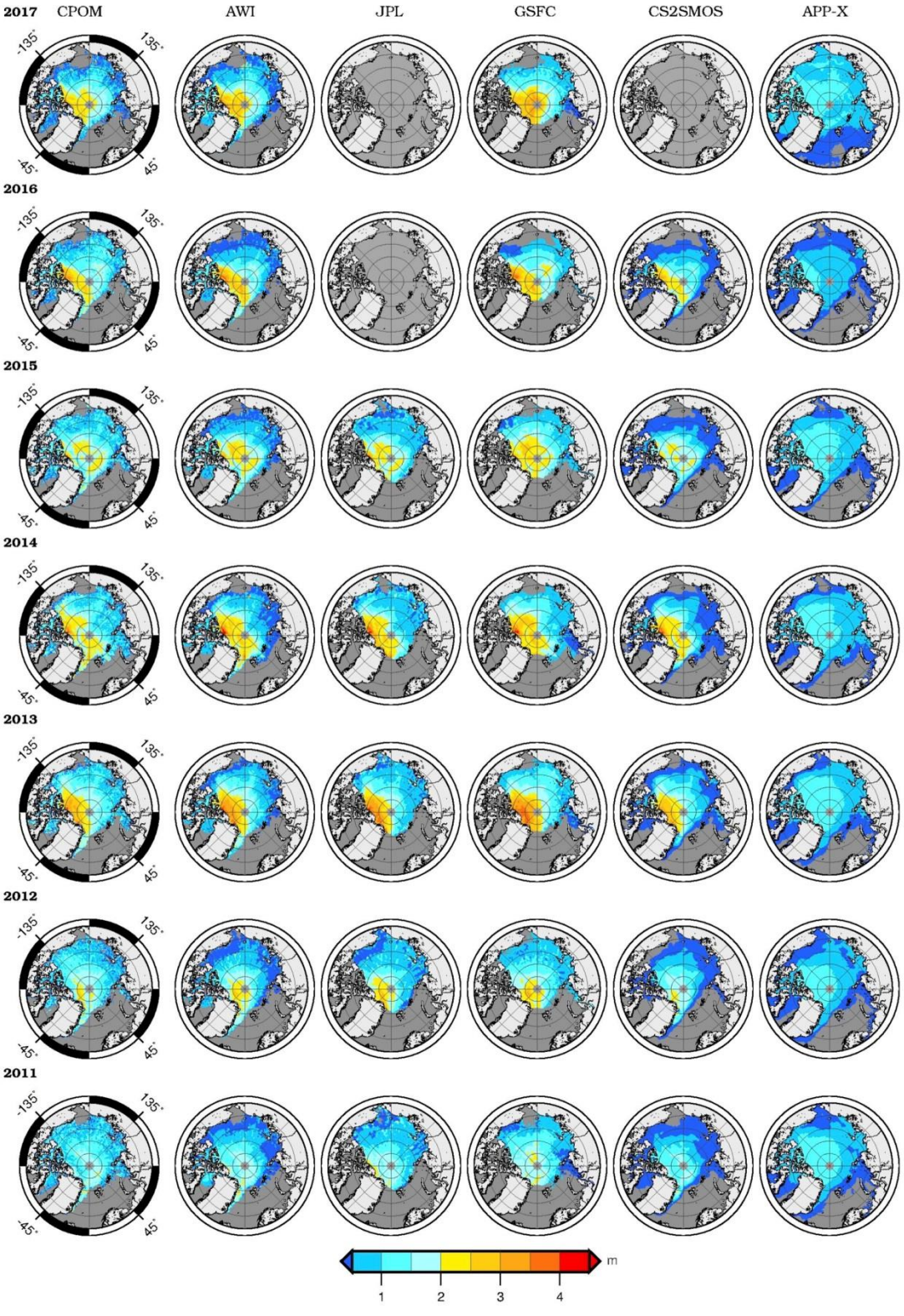

The Cryosphere Discuss., https://doi.org/10.5194/tc-2018-197
Manuscript under review for journal The Cryosphere
Discussion started: 24 September 2018

(b)

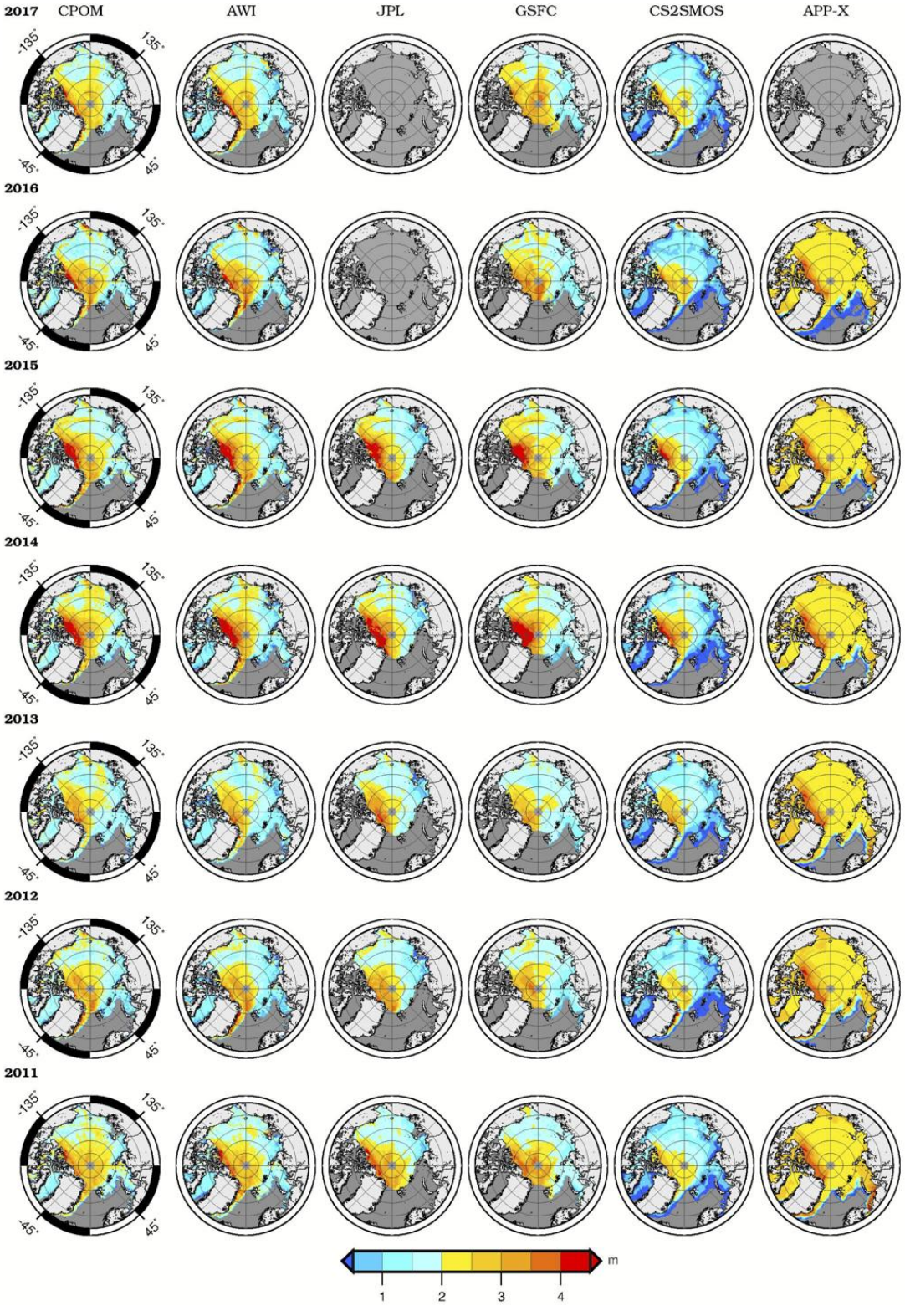

The Cryosphere Discuss., https://doi.org/10.5194/tc-2018-197
Manuscript under review for journal The Cryosphere
Discussion started: 24 September 2018

Figure 2: Maps of seasonally-averaged sea ice thickness for each product over the period 2011–2017, for (a) October–November, and (b) March–April.

The Cryosphere Discuss., https://doi.org/10.5194/tc-2018-197
Manuscript under review for journal The Cryosphere
Discussion started: 24 September 2018

(a)

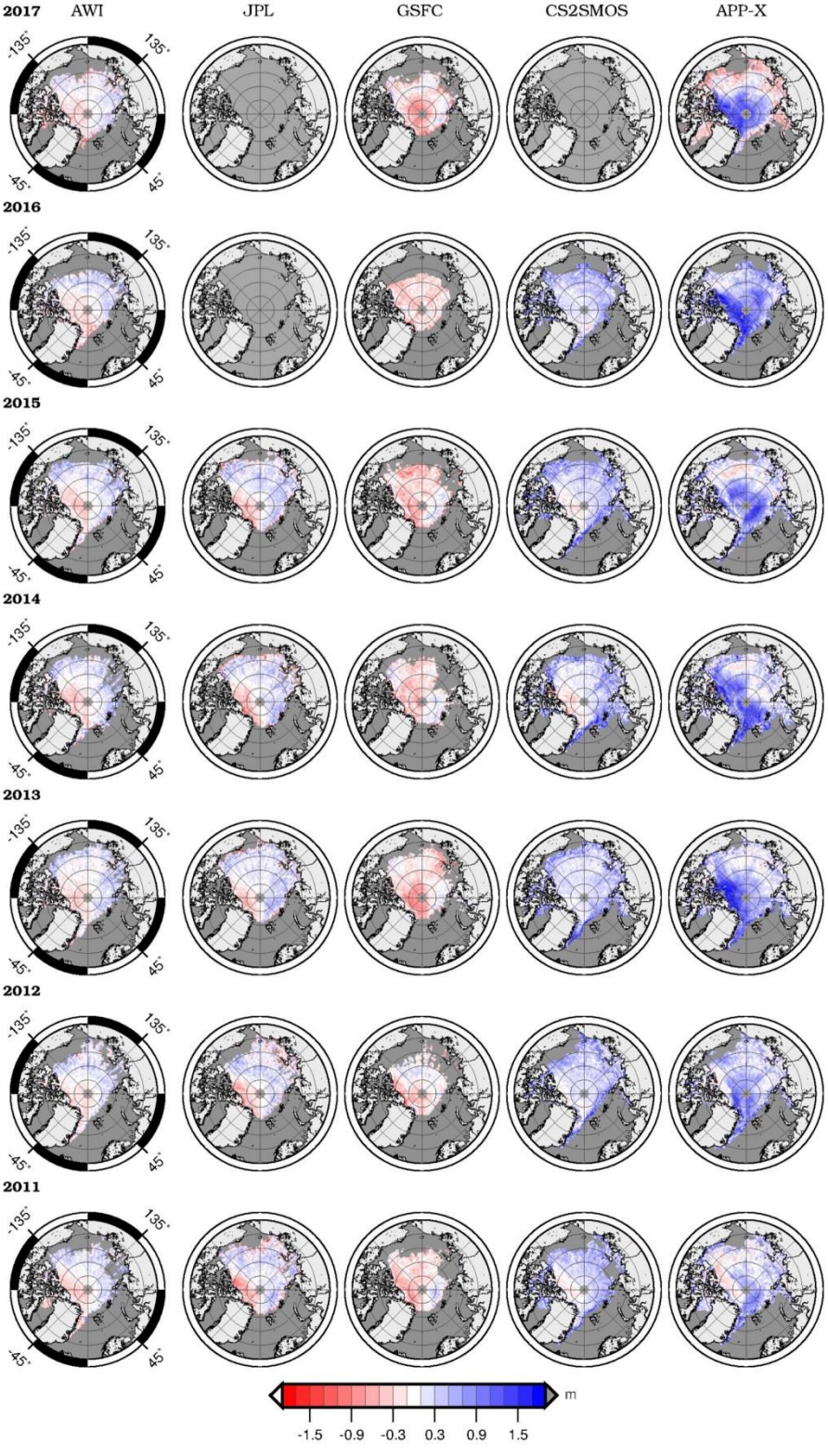

The Cryosphere Discuss., https://doi.org/10.5194/tc-2018-197
Manuscript under review for journal The Cryosphere
Discussion started: 24 September 2018

(b)

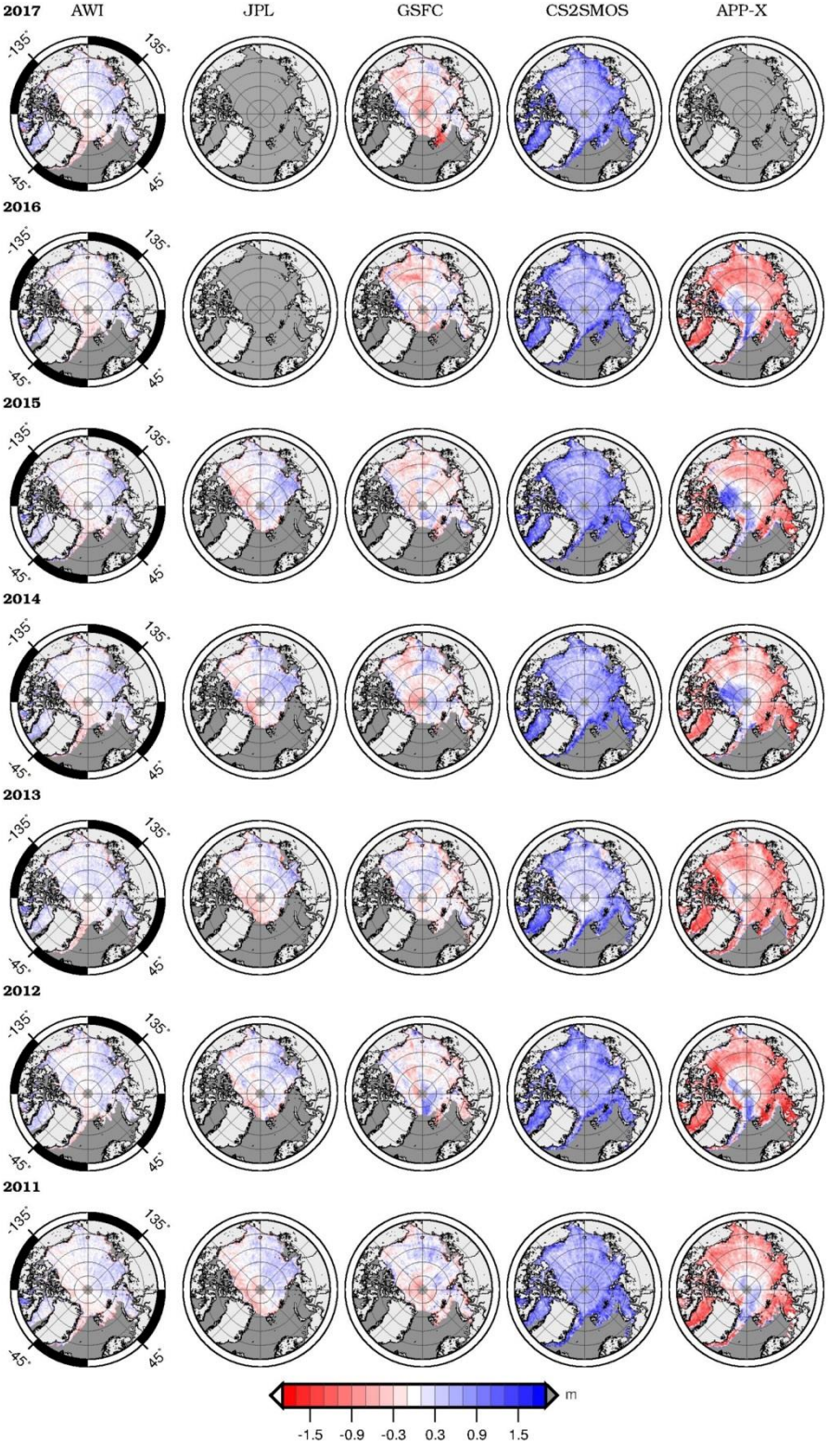

The Cryosphere Discuss., https://doi.org/10.5194/tc-2018-197
Manuscript under review for journal The Cryosphere
Discussion started: 24 September 2018

Figure 3: Maps of seasonally-averaged sea ice thickness differences for the period 2011–2017, where each data product is subtracted from the reference data set (CPOM), for (a) October–November and (b) March–April. Red (blue) regions indicate areas where the seasonally-averaged thickness is greater (less) than the reference data product.

The Cryosphere Discuss., https://doi.org/10.5194/tc-2018-197
Manuscript under review for journal The Cryosphere
Discussion started: 24 September 2018

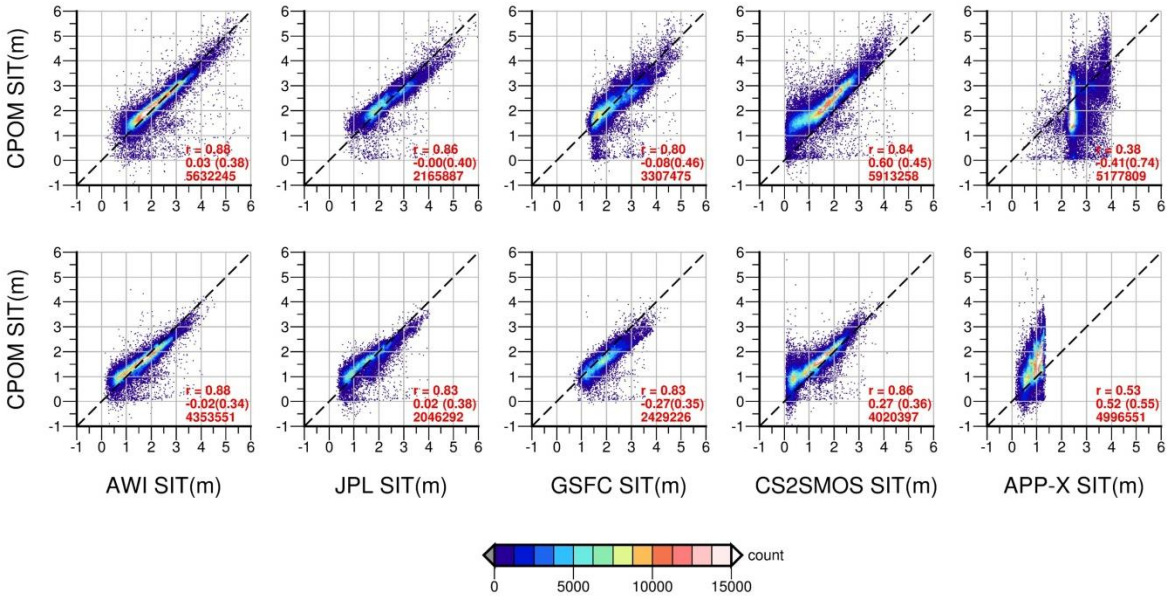

Figure 4: Sea ice thickness for each product compared to the reference data set for March–April (top) and October–November (bottom). Colour indicates measurement density, derived from the number of data points within each 0.05 m cell. Statistics for correlation (r), mean difference (std. dev.), and number of data points are provided. The period over which correlations are calculated is based on product availability, as outlined in Table 1.

The Cryosphere Discuss., https://doi.org/10.5194/tc-2018-197
Manuscript under review for journal The Cryosphere
Discussion started: 24 September 2018

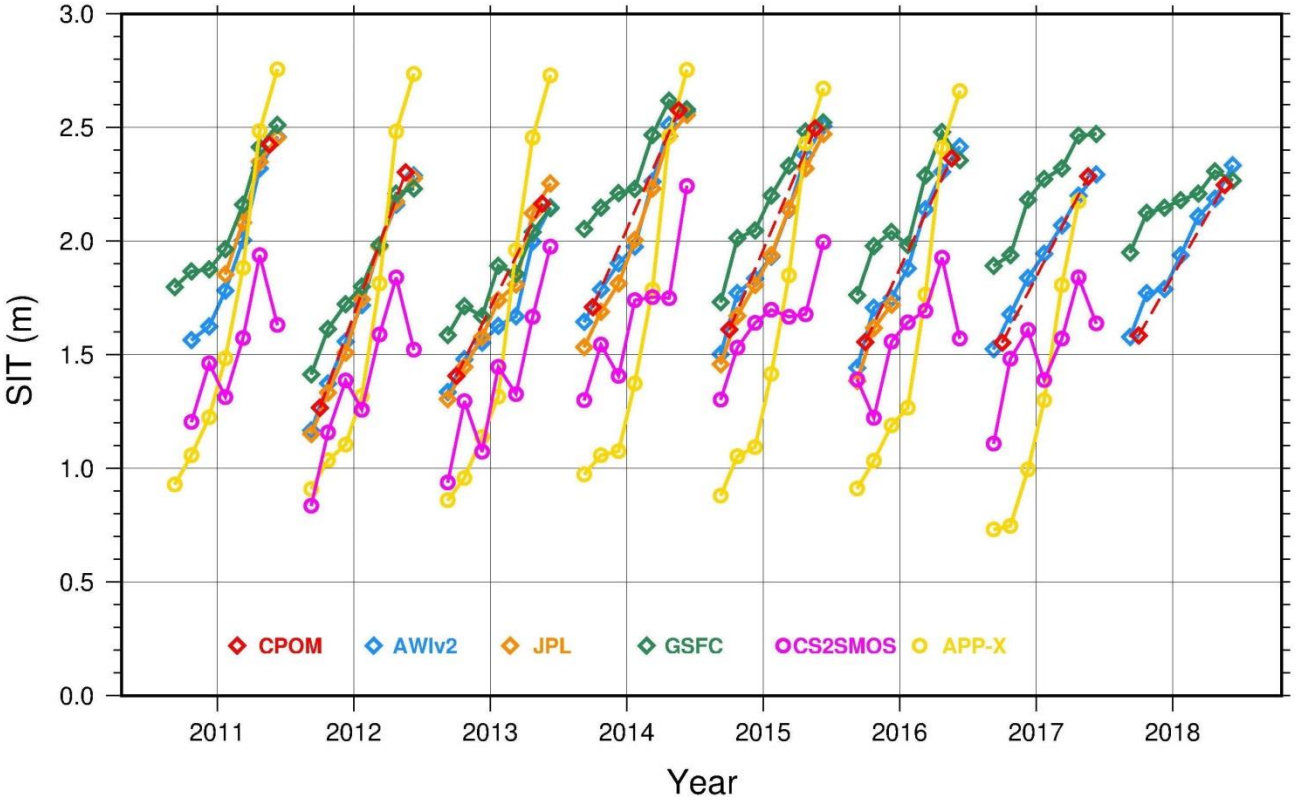

Figure 5: Sea ice thickness growth curves for October–April (monthly averages) during the period 2010–2018, for each product per availability (solid lines), indicating interannual variability in the winter-time thickness evolution. For CPOM data, only the October–November and March–April seasonal averages are shown, connected by a dashed red line.

The Cryosphere Discuss., https://doi.org/10.5194/tc-2018-197
Manuscript under review for journal The Cryosphere
Discussion started: 24 September 2018

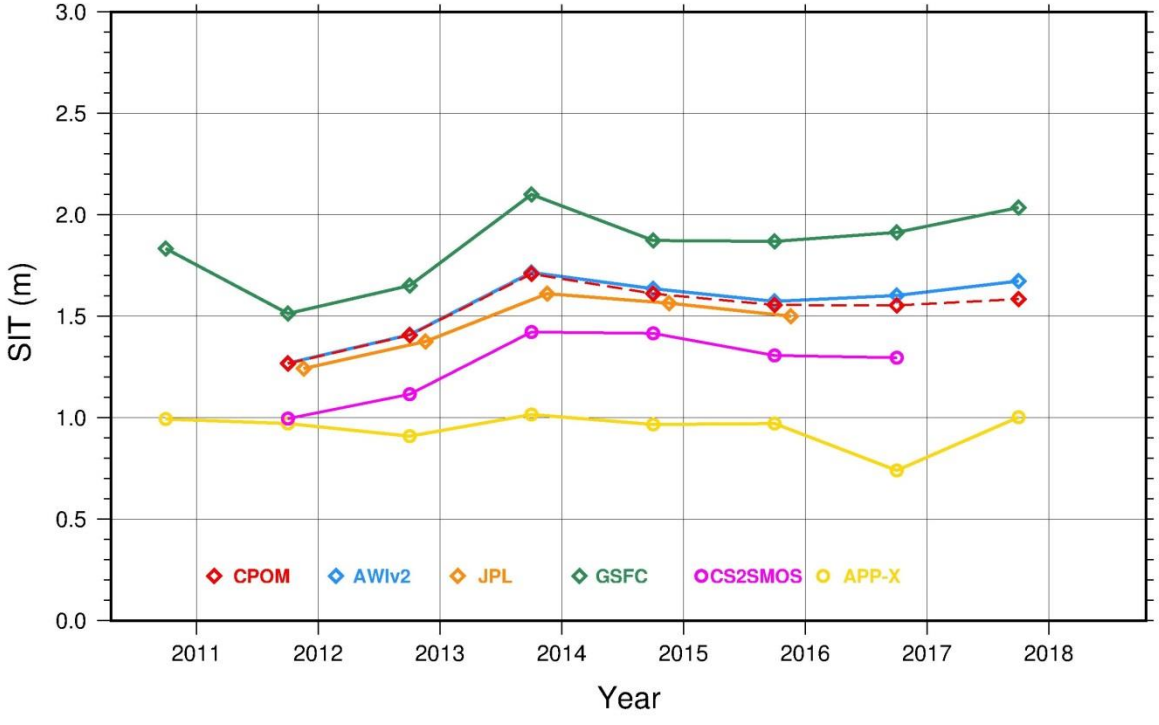

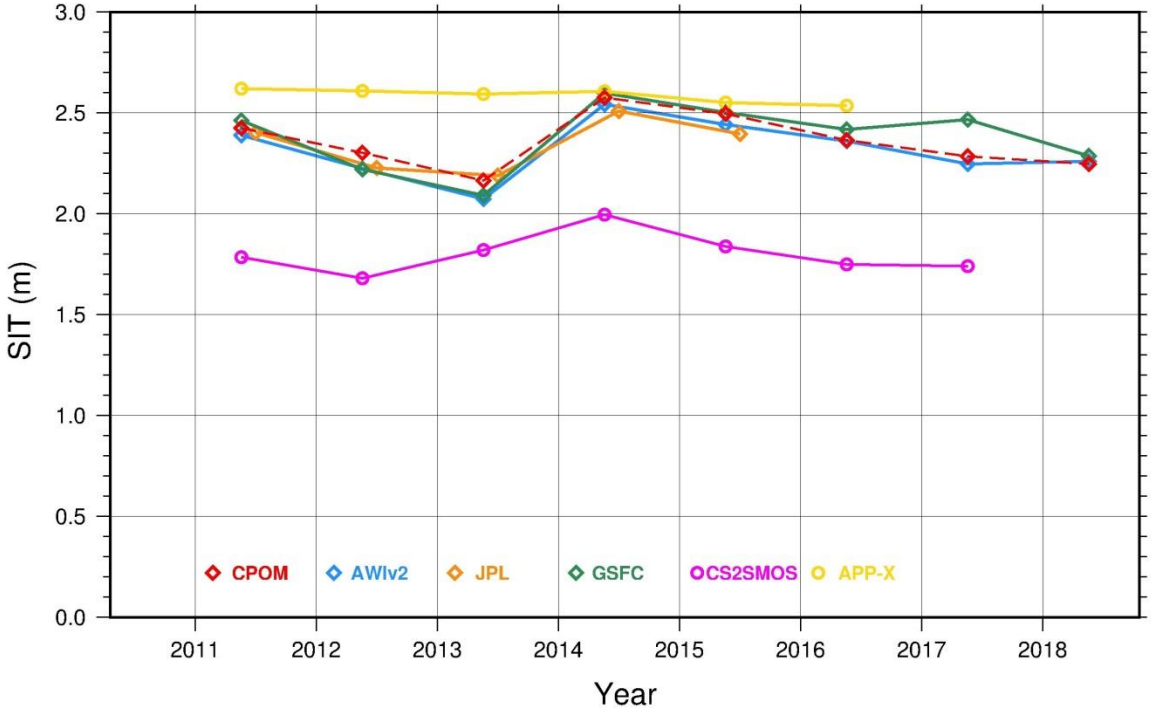

Figure 6: Time series of seasonally-averaged sea ice thickness for each product, for (a) October–November, and (b) March–April, over the central Arctic (regions 1–6) during the period 2010–2018, based on product availability as outlined in Table 1.

The Cryosphere Discuss., https://doi.org/10.5194/tc-2018-197
Manuscript under review for journal The Cryosphere
Discussion started: 24 September 2018

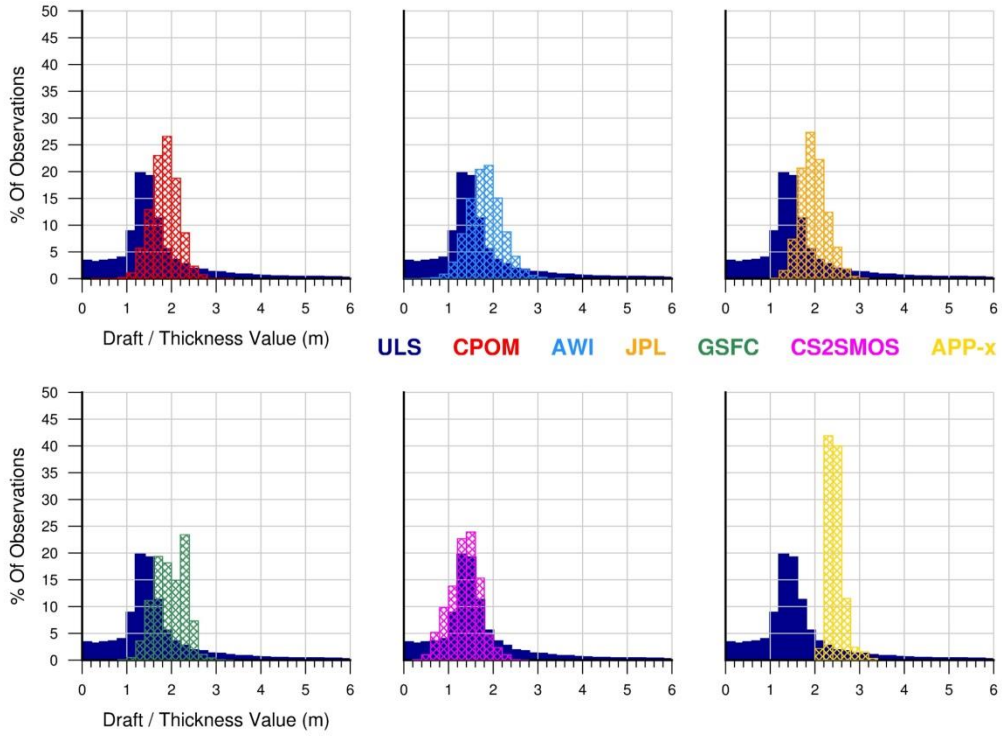

Figure 7: Spring (March–April) sea ice thickness distributions (cross-hatched) for each data product within 200 km radius of BGEP mooring locations, averaged for the period 2011 to 2016, overlaid on the corresponding BGEP upward looking sonar (ULS) ice draft distribution (dark blue, solid). Histogram bin width is 0.2 m.

The Cryosphere Discuss., https://doi.org/10.5194/tc-2018-197
Manuscript under review for journal The Cryosphere
Discussion started: 24 September 2018

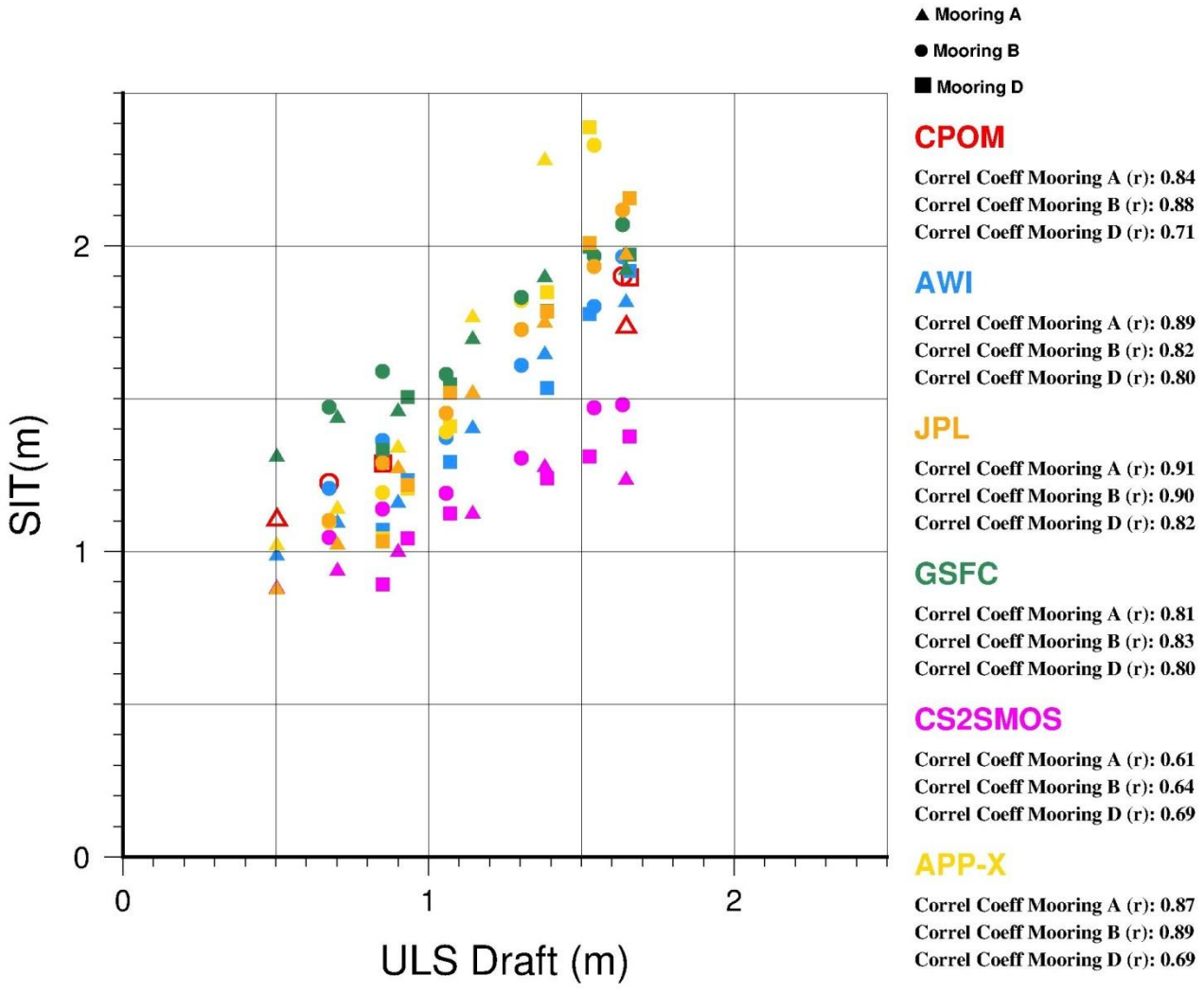

Figure 8: Correlation between monthly-averaged, satellite-derived ice thickness and ULS ice draft, for six months spanning November to April. Correlation coefficients are provided per ULS mooring (locations indicated by symbols), for the period 2010–2016, with the exception of the JPL product, wherein monthly averages and correlation coefficients are calculated for the period 2011–2015. In the case of the CPOM product the correlation coefficients are calculated based on seasonal (October–November, March–April) rather than monthly averages. Here, monthly averages were further combined across years (e.g. November 2011–2016, December 2011–2016, etc.) to provide six data points per mooring-product comparison.

The Cryosphere Discuss., https://doi.org/10.5194/tc-2018-197
Manuscript under review for journal The Cryosphere
Discussion started: 24 September 2018

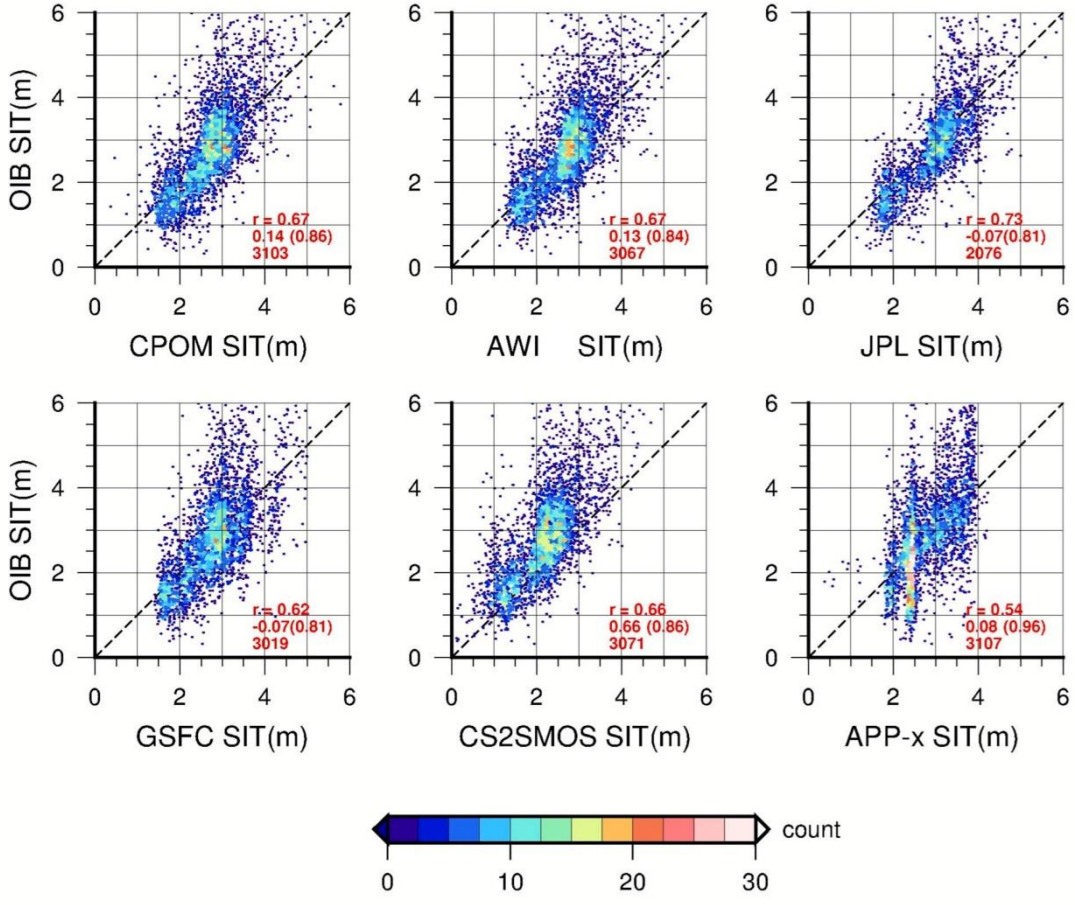

Figure 9: Comparison of satellite-derived ice thickness with Operation IceBridge thickness estimates at the end of the winter growth season (March–April). Comparisons were conducted by gridding satellite and aircraft data onto a common 50 km grid and using grid cells in which both data sets contained thickness estimates. Colour indicates measurement density (number of data points within each 0.01 m cell). Statistics for correlation (r), mean difference (std. dev.), and number of data points are calculated for the period 2011–2017, with the exception of the JPL product, wherein statistics are calculated for the period 2011–2015.

The Cryosphere Discuss., https://doi.org/10.5194/tc-2018-197
Manuscript under review for journal The Cryosphere
Discussion started: 24 September 2018

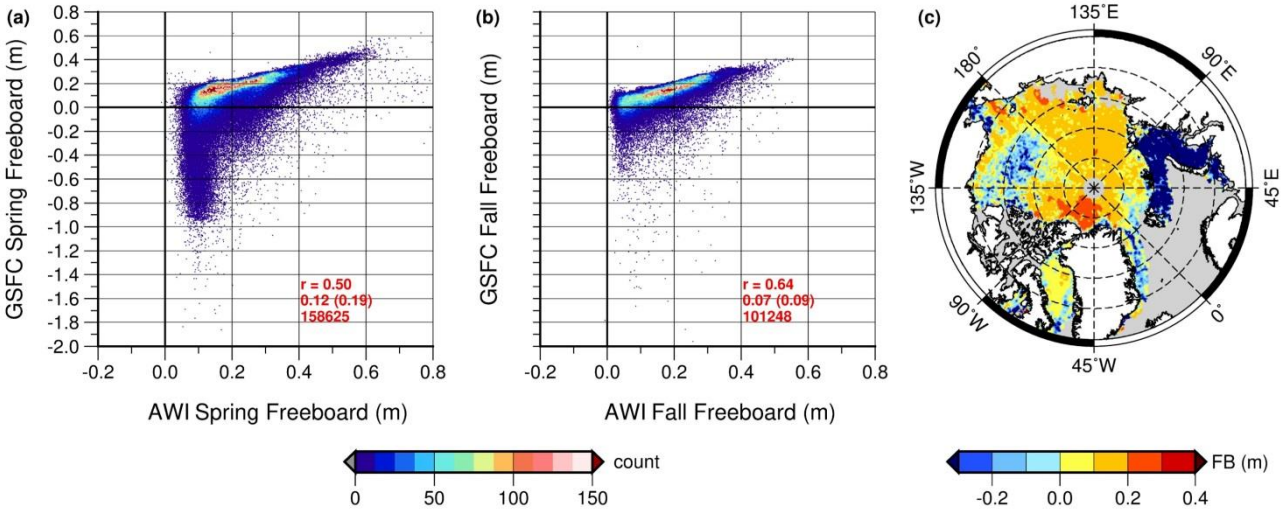

Figure 10: Comparison of sea ice freeboard in the GSFC and AWI data products for (a) March–April and (b) October–November, for the period 2011–2018. Data were gridded at 25 km and data common to both grids were compared. Colour indicates measurement density, derived from the number of data points within each 0.01 m cell. Statistics for correlation (r), mean difference (std. dev.), and number of data points are provided. (c) GSFC product freeboard (FB) for April 2014.

The Cryosphere Discuss., https://doi.org/10.5194/tc-2018-197
Manuscript under review for journal The Cryosphere
Discussion started: 24 September 2018

Table 1. Characteristics of satellite-derived ice thickness products (quality flag refers to the availability of a thickness uncertainty estimate or quality flag). Latency is the difference between the date of data acquisition and data delivery, estimated from data portal time stamps at the time of writing. Frequency refers to the temporal offset between consecutive datasets (e.g. daily, weekly, monthly).

Product Name	CPOM	AWI	NASA / JPL	NASA / GSFC	CS2SMOS	APP-x
Temporal Range	March 2011–date (October–April only)	November 2010–date	January 2011–December 2015	October 2010–date	November 2010–April 2017	January 1982–date
Frequency	Daily (NRT) / seasonally	Monthly	Not updated post 2015	Daily	Weekly	Twice daily
Geograpical Coverage (by region number)	(1)–(14), full Northern Hemisphere	(1)–(14), poleward of 60 ºN	(1)–(6)	(1)–(8), (10, partial)	(1)–(14), poleward of 50 ºN	(1)–(14), poleward of 50 ºN
Averaging Period	NRT data product: 2, 14, 28 days. Seasonally-averaged product: 2 months	1 month	1 month	30 day	7 day	12 hours
Latency	3 days (NRT) / seasonally	Variable	Not updated post 2015	~6 weeks	Variable	~4 days (as of April 2018)
Grid Resolution	25 km, 5 km (full Arctic), 1 km (individual regions)	25 km	25 km	25 km	25 km	25 km (EASE grid)
Freeboard	No	Yes	No	Yes	No	No
Quality Flag	No	Yes	No	No	Yes	No
Technique	70% Threshold First Maxima Retracker Algorithm (TFMRA)	50% TFMRA	Waveform centroid retracker	Waveform fitting	Blended SMOS and CS2 data	One-dimensional Thermodynamic Ice Model (OTIM)
Mean Sea Surface	UCL2013	DTU15 MSS	EGM2008 geoid	DTU10 MSS	DTU15 MSS (for CS-2 data)	N/A
Snow Depth	Modified Warren Climatology	Modified Warren Climatology	Modified Warren Climatology	Modified Warren Climatology	Modified Warren climatology (CS2 data); linear relation with ice thickness (SMOS data)	0.2 m
Ice Density	FYI: 916.7 kg/m^3; MYI: 882.0 kg/m^3	FYI: 916.7 kg/m^3; MYI: 882.0 kg/m^3	FYI: 917 kg/m^3; MYI: 882.0 kg/m^3	915 kg/m^3	FYI: 916.7 kg/m^3; MYI: 882.0 kg/m^3	N/A
Ice Concentration, Threshold	NSIDC Near-Real-Time DMSP SSMIS Daily Polar Gridded Sea Ice Concentrations, 75%	OSI-SAF, 70%	Not specified	NSIDC Near-Real-Time DMSP SSMIS Daily Polar Gridded Sea Ice Concentrations, 70%	OSI-SAF, 15%	NSIDC Nimbus-7 SMMR and DMSP SSM/I passive microwave data with NASA Team Algorithm applied, 15%
Ice Type	OSI-SAF	OSI-SAF	ASCAT	OSI-SAF	OSI-SAF	Converted from reflectances
References	Laxon et al., 2013; Tilling et al., 2016	Ricker et al., 2014; Hendricks et al., 2016	Kwok and Cunningham, 2015	Kurtz et al., 2014; Kurtz and Harbeck, 2017	Tian-Kunze et al., 2014; Kaleschke et al., 2015, Ricker et al., 2016	Wang et al., 2010; Key and Wang, 2015; Wang et al. 2016
Public Data Source	http://www.cpom.ucl.ac.uk/csopr/seaice.html	Meereisportal, http://data.meereisportal.de/ (Grosfeld et al. 2016)	https://rkwok.jpl.nasa.gov/cryosat/download.html	https://nsidc.org/data/RDEFT4	Meereisportal, http://data.meereisportal.de/ (Grosfeld et al. 2016)	https://www.ncei.noaa.gov/data/avhrr-polar-pathfinder-extended/access/nhem/

The Cryosphere Discuss., https://doi.org/10.5194/tc-2018-197
Manuscript under review for journal The Cryosphere
Discussion started: 24 September 2018

Table 2. Seasonally-averaged sea ice thickness for each Arctic region (in meters) for all six data products, where ice cover was greater than 10%. Regional averages are calculated over the period 2011–2017, but are based on product availability, as outlined in Table 1.

	October–November						March–April					
	CPOM	**AWI**	**JPL**	**GSFC**	**CS2SMOS**	**APP-x**	**CPOM**	**AWI**	**JPL**	**GSFC**	**CS2SMOS**	**APP-x**
Arctic Ocean [1]	1.64	1.75	1.6	2.03	1.44	1.01	2.46	2.42	2.45	2.5	1.93	2.6
Lincoln Sea [2]	2.04	2.13	2.58	2.45	1.99	1.18	3.8	3.65	3.68	3.39	2.94	3.64
Beaufort Sea [3]	1.01	1.04	1.06	1.5	0.66	0.89	2.06	1.99	2.1	2.04	1.31	2.6
Chukchi Sea [4]	-	-	-	-	-	-	1.95	1.83	1.82	1.94	1.18	2.51
East Siberian Sea [5]	0.91	0.76	0.82	1.27	0.4	0.67	1.8	1.7	1.59	1.74	1.14	2.44
Laptev Sea [6]	0.81	0.52	0.69	0.99	0.35	0.61	1.5	1.25	1.15	1.55	0.78	2.4
Kara Sea [7]	-	-	-	-	-	-	1.6	1.39	-	1.56	0.69	2.49
Barents Sea [8]	-	-	-	-	-	-	1.45	1.45	-	1.67	0.38	2.3
Greenland Sea [10]	1.68	1.89	-	-	1.14	0.75	2.62	3.04	-	-	1.7	2.39
Baffin Bay [11]	-	-	-	-	-	-	1.53	1.26	-	-	0.54	2.48
Davis Strait [12]	-	-	-	-	-	-	1.59	1.21	-	-	0.48	2.7
Hudson Strait [13]	-	-	-	-	-	-	1.49	0.81	-	-	0.44	2.91
Canadian Archipelago [14]	1.29	1.42	-	-	0.85	0.92	1.97	1.44	-	-	1.32	2.66

The Cryosphere Discuss., https://doi.org/10.5194/tc-2018-197
Manuscript under review for journal The Cryosphere
Discussion started: 24 September 2018

Table 3. Deviation of seasonally-averaged annual sea ice thickness (in meters) from the seasonally-averaged climatological mean within the central Arctic (regions 1–6). The climatological mean is calculated per product availability during the period 2011–2017 (i.e. the JPL product climatological mean is calculated for the period 2011–2015, while the fall CS2SMOS and spring APP-x product climatological means are calculated for the period 2011–2016).

March–April	**2011**	**2012**	**2013**	**2014**	**2015**	**2016**	**2017**
CPOM	0.05	−0.07	−0.21	0.2	0.12	0	−0.09
AWI	0.06	−0.10	−0.25	0.22	0.12	0.04	−0.09
JPL	0.06	−0.11	−0.15	0.16	0.05	-	-
GSFC	0.07	−0.18	−0.30	0.21	0.11	0.02	0.07
CS2SMOS	−0.02	−0.12	0.02	0.2	0.04	−0.05	−0.07
APP-x	0.03	0.02	0.01	0.02	−0.04	−0.05	-
October–November	**2011**	**2012**	**2013**	**2014**	**2015**	**2016**	**2017**
CPOM	−0.27	−0.12	0.2	0.07	0.03	0.02	0.04
AWI	−0.34	−0.18	0.22	0.07	0.06	0.02	0.14
JPL	−0.24	−0.09	0.18	0.11	0.05	-	-
GSFC	−0.40	−0.25	0.36	0.02	0.03	−0.01	0.25
CS2SMOS	−0.30	−0.16	0.21	0.18	0.07	0	-
APP-x	0.04	−0.03	0.08	0.03	0.04	−0.21	0.04

The Cryosphere Discuss., https://doi.org/10.5194/tc-2018-197
Manuscript under review for journal The Cryosphere
Discussion started: 24 September 2018

Table 4. Annual winter (January–April*) sea ice draft/thickness (meters, top value) and deviation from the climatological average (meters, bottom value) for each BGEP ULS mooring (A, B, D) and five satellite products (using measurements within 200 km of BGEP moorings). Climatological mean is calculated per product for the period 2011–2016. *March–April for CPOM statistics.

		ULS	CPOM	AWI	JPL	GSFC	CS2SMOS	APP-x
Mooring A	**2011–2016**	1.27	1.74	1.51	1.61	1.75	1.17	1.99
	2011	1.15 -0.12	1.70 -0.04	1.4 -0.11	1.45 -0.16	1.5 -0.25	1.12 -0.04	2.01 0.02
	2012	1.39 0.12	1.75 0.01	1.43 -0.09	1.42 -0.19	1.68 -0.07	0.96 -0.2	2.04 0.05
	2013	1.05 -0.22	2.06 0.32	1.51 0.0	1.61 -0.01	1.48 -0.27	1.16 -0.01	2.02 0.03
	2014	1.51 0.24	2.12 0.37	1.71 0.2	1.85 0.24	2.09 0.34	1.41 0.25	1.96 -0.03
	2015	1.32 0.05	2.13 0.39	1.73 0.21	1.74 0.12	2.09 0.34	1.38 0.21	1.99 0.0
	2016	1.2 -0.07	1.61 -0.13	1.3 -0.22	-	1.67 -0.08	0.96 -0.21	1.91 -0.08
		ULS	**CPOM**	**AWI**	**JPL**	**GSFC**	**CS2SMOS**	**APP-x**
Mooring B	**2011–2016**	1.38	1.9	1.69	1.78	1.86	1.36	2.02
	2011	1.42 0.04	1.90 - 0.01	1.61 -0.08	1.61 -0.17	1.61 -0.25	1.27 -0.09	2.03 0.02
	2012	1.4 0.02	1.89 -0.01	1.67 -0.01	1.72 -0.07	1.7 -0.16	1.3 -0.06	2.06 0.05
	2013	1.2 -0.19	2.04 0.14	1.77 0.08	1.83 0.04	1.75 -0.11	1.51 0.15	2.03 0.02
	2014	1.47 0.09	2.02 0.12	1.77 0.09	1.85 0.06	2.09 0.23	1.53 0.17	1.98 -0.04
	2015	1.55 0.17	2.02 0.12	1.83 0.14	1.92 0.14	2.06 0.2	1.41 0.05	2.02 0.0
	2016	1.26 -0.13	1.55 -0.36	1.47 -0.22	-	1.95 0.09	1.14 -0.22	1.96 -0.05
		ULS	**CPOM**	**AWI**	**JPL**	**GSFC**	**CS2SMOS**	**APP-x**
Mooring D	**2011–2016**	1.41	1.9	1.63	1.81	1.82	1.26	2.08
	2011	1.48 0.07	1.70 -0.20	1.48 -0.15	1.54 -0.27	1.66 -0.16	1.15 -0.11	2.15 0.07
	2012	1.39 -0.02	1.75 -0.14	1.51 -0.12	1.6 -0.21	1.66 -0.16	1.12 -0.14	2.15 0.06
	2013	1.06 -0.35	2.06 0.16	1.51 -0.12	1.59 -0.21	1.55 -0.27	1.18 -0.08	2.16 0.08
	2014	1.64 0.23	2.12 0.22	1.89 0.26	2.13 0.33	2.15 0.32	1.55 0.29	2.09 0.01
	2015	1.59 0.18	2.13 0.24	1.97 0.34	2.16 0.36	2.26 0.43	1.57 0.31	2.0 -0.08
	2016	1.31 -0.1	1.61 -0.28	1.42 -0.21	-	1.67 -0.15	0.99 -0.27	1.95 -0.14